GFAP Degradation in TBI:

Linking Novel Modified Products to Astrocyte Pathology and Patient Outcome

Ina-Beate Wanner[1*], Julia Halford[1], Jonathan Lopez[1], Sean Shen[2], Yu Chen[3], Hayden Zhao[1], Carolina Salas[1], Rachel R. Ogorzalek Loo[2], Steven Robicsek[4], Benjamin M. Ellingson[5], Jeffrey Gornbein[6], Timothy E. Van Meter[7], Gerry Shaw[8,9], Joseph A. Loo[2], and Paul M. Vespa[10].

Author affiliations:

2: Dept. of Chemistry and Biochemistry, Molecular Biology Institute, David Geffen School of Medicine, UCLA, Los Angeles, CA, USA.
3: Molecular Instrumentation Center (MIC), Dept. of Chemistry and Biochemistry, UCLA, Los Angeles, CA, USA.
4: Dept. of Anesthesiology, Neurosurgery and Neuroscience, University of Florida, Gainesville, FL 32610-0254, USA.
5: Dept. of Radiological Sciences, Geffen S
chool of Medicine, UCLA, Los Angeles, CA, USA.
6: Dept. of Computational Medicine, Statistics Core of the Dept of Medicine, School of Public Health, UCLA, Los Angeles, CA, USA.
7: BRAINBox Solutions, Inc., Richmond, VA 23219, USA.
8: Dept. of Neuroscience, University of Florida College of Medicine, Gainesville, FL 32610, USA.
9: EnCor Biotechnology Inc., Gainesville, FL, 32608, USA.
10: Dept. Neurology and Neurosurgery, BIRC; David Geffen School of Medicine, Ronald Reagan Medical Center, UCLA, Los Angeles, CA, USA.

Correspondence to: Ina-Beate Wanner
1: Semel Institute for Neuroscience and Human Behavior, Intellectual and Developmental Disability Center (IDDRC); Brain Injury Research Center (BIRC); 635 Charles E. Young Drive South, NRB315, David Geffen School of Medicine, UCLA, Los Angeles, CA 90095, USA;
Primary email: IWanner@mednet.ucla.edu Alternative email: iwanner@g.ucla.edu

Running title: GFAP degradome and astrocyte pathology in TBI

Keywords: neurotrauma, pathomechanism, neurodegeneration, biomarker profiling, proteostasis, monitoring

ABSTRACT

Glial fibrillary acidic protein (GFAP) is an important clinical biomarker of traumatic brain injury (TBI), yet understanding the nature, timing, and impact of its degraded and modified products is needed for clinical utility. We report distinct GFAP breakdown products (BDPs) and post-translational modifications (PTMs) that are unique to TBI. Mapped PTMs provided fragment and patient-specific citrullination signatures known for destabilizing GFAP filaments. GFAP and its fragments from patients' cerebrospinal fluid (CSF) and serum were sequenced by mass spectrometry (MS), identifying two TBI-specific coproducts covering coil1 (20-26kDa) and coil2 (15-19kDa) in the rod-domain. These coproducts were imbalanced in biofluids with coil1-BDP enriched over coil2-BDPs detected by label-free quantitative MS and independently confirmed by immunoblot densitometry in twenty-three TBI patients. Ten-day temporal trajectories showed ongoing proteolysis, progressing from large to small fragments, with prolonged elevation of 37/39kDa fragments, and delayed rise of small products. For the first time, profiles of GFAP fragments, but not of uncleaved GFAP, predicted six-month outcome (Extended Glasgow Outcome Scale, GOSE), highlighting proteolytic processing as prognostic biomarker signature. These new TBI-GFAP-BDPs were independently substantiated in a human culture trauma model, offering mechanistic insight. To this end, specific findings include: Coil1-BPDs were fluid-released, while coil2-BDPs remained cellular, shown by epitope-defined coil-specific GFAP antibodies. A new cleavage site between the two coils was identified by selective epitope loss. Coil2's cellular retention could be explained by incorporation of citrullinated coil2-BDPs into non-filamentous aggregates within pathological astrocytes. Trauma-triggered proteolysis involved calpains and caspases in distinct astrocyte injury states documented using inhibitors and live-cell reporters. These novel degradation findings have significant translational relevance for monitoring disease progression in TBI patients and for linking biofluid GFAP fragments to a trauma-inflicted astroglial proteinopathy during neurodegeneration.

INTRODUCTION

Traumatic brain injury (TBI) affects 56 million people worldwide annually; nearly one in five U.S. adults have a lifetime history of TBI, making it the most common neurological disorder [68, 94]. More than half of mild TBI and 85% of moderate-to-severe patients fail to achieve long-term recovery [108, 109]. TBI nearly doubles the lifetime risk (22-29%) for neurodegenerative disease, a public health challenge that grows as populations age [99]. While the link between TBI and dementia is established, molecular mechanisms underlying this progression are less clear [140]. Early detection of brain-altering protein changes after TBI is essential and depends on sensitive biomarkers. Defining early-stage TBI pathological proteoforms associated with biomarkers will facilitate risk assessment to capture emerging signatures that may develop into post-TBI neurodegeneration [20, 99].

A pathological hallmark of neurodegenerative disease is accumulation of toxic proteoforms resulting from maladapted protein homeostasis, including amplified protein posttranslational modifications (PTMs) and

degradation [51, 129, 162]. Deranged proteostasis is also a prominent consequence of TBI, triggered by rapid and sustained calcium elevation initiated by membrane disruption and excitotoxicity. Increased proteolysis with rapid postinjury activation of calpains and caspases are well-documented in pre-clinical TBI models [10, 14, 34, 134, 169]. While tau, ß-amyloid and α-synuclein proteinopathies are known in neurodegeneration and TBI, deranged proteostasis plausibly affects many more proteins. Linking evolving neurodegenerative processes with a diagnostic signature requires understanding the relationship between cell and biofluid proteoforms. While imaging and postmortem studies can confirm advanced proteinopathies, tools to monitor their early initiation after TBI remain underdeveloped. As proteolysis and altered PTMs emerge from early TBI pathophysiology, their study and detection are critical for evaluating pathogenic conversion and recovery [47, 112].

Two strategies that may capture a pathological conversion of TBI toward neurodegeneration are: 1) linking early-elevated TBI biomarkers to neuropathology [123], or 2) investigating pathological changes in TBI biomarkers themselves. Post-injury calpain and caspase activation is often reported using αII-spectrin breakdown products (SBDPs), but their translation into clinically useful biomarkers is limited due to its ubiquitous expression [95, 126, 131, 144]. In contrast, astroglial intermediate filament glial fibrillary acidic protein (GFAP) is highly brain-enriched and extensively studied as a TBI biomarker: GFAP fluid levels are elevated with intracranial injuries [12, 103, 120]. Circulating fluid GFAP levels rise fast, peak 6-18h postinjury, and then decline [54, 119, 121, 132]. Elevated serum GFAP predicts poor outcome and mortality [93, 122, 132, 160]. GFAP blood testing is FDA approved within a narrow context of use (COU) on the injury day [12, 116], and is incorporated into the new National Institute of Neurological Disorders and Stroke (NINDS) TBI classification framework, reflecting its growing role in clinical TBI evaluation [13, 98]. While well-established as an acute diagnostic biomarker, longitudinal monitoring of altered GFAP proteoforms and their possible use to indicate deranged proteostasis remain open priorities [37, 146, 158].

GFAP breakdown products (BDPs) are in biofluids after TBI and commercial GFAP assays include their detection, yet TBI-specific fragment sequences and their degradation kinetics are undefined [54, 100, 173]. Can pathological GFAP-BDP proteolysis be tracked after TBI? What connects GFAP biomarker signals to proteinopathy? The mechanistic link between biofluid GFAP and its astroglial proteoforms is unknown, beginning with the puzzle of the acute release of a cytoskeleton-tethered protein [124]. In neuropathology, GFAP upregulation is widely used as a reactive astrogliosis indicator, yet trauma-release occurs faster than de novo expression [58, 101, 142]. GFAP modification, misfolding, and degradation have detrimental consequences for astrocytes [88, 101, 117]. Those consequences are critical because astrocytes are indispensable for intact neurovascular coupling, integrity of the blood-brain barrier, metabolite support, neural network function and memory formation. Astrocyte degeneration and their injury states after trauma are just beginning to be acknowledged [54, 107, 170]. The relevance of GFAP proteinopathy is underscored by Alexander disease, a progressive neurodegenerative disease that is causally linked to toxic GFAP aggregates initiated by mutations and fragmentation with elevated biofluid GFAP [6, 35, 57, 63, 89, 102, 118]. Clarifying GFAP degradation and modification in both TBI biofluids and injured astrocytes is critical to improving biomarker interpretation and outcome prediction.

To start bridging these translational gaps, we performed deep proteomic sequencing of immunopurified GFAP fragments in TBI patient cerebrospinal fluid (CSF) validated by GFAP-BDP profiling in a cohort of TBI patients. These studies established the trajectory GFAP proteolysis after TBI and that temporal degradation is predictive of outcome release of unmodified GFAP. Patient findings were then mechanistically explored using a unique human trauma culture model. This work confirms trauma-specific fragments and modifications, identifies trauma cleavage, documents distinct product distribution fates and connects fluid GFAP elevation with modified GFAP aggregation in traumatized astrocytes. These findings advance the molecular understanding of GFAP degradation dynamics post-TBI and contribute to detecting neurodegeneration-associated pathological features after neurotrauma.

MATERIALS AND METHODS

TBI patients' demographic and clinical data and brain tissue specimen procurement

This observational DANA foundation funded cohort study included 112 CSF samples and 3 serum samples from 26 consented adult TBI patients admitted to neurocritical care at level one trauma centers at UCLA and at the University of Florida, Gainesville, and a commercial control serum sample (Precision Med; Supplement Tables S1, S2). Patient median age was 40±19 years, 22 subjects were male and 4 were female, and median score on the Glasgow Coma Scale (GCS) was 6 ±3.4. Enrollment occurred between 2018-2023 and included anonymous demographic and clinical parameters (Supplement Table S1). All except two patients had recovery scores on the Glasgow Outcome Scale (GOS) reported both at hospital discharge and by phone interview at six-month postinjury on extended GOS (GOSE). Deidentified human fetal brain tissue from voluntarily aborted pregnancies was donated adhering to stringent ethical regulations. See Declarations for Ethics approval statements on all with consent donated human specimen at the end. Cerebral astrocyte cultures were prepared from donated human fetal cranial specimen aged 16-19.5 gestational weeks.

Immunoprecipitation and mass spectrometry sequencing of GFAP from TBI patients

Mass spectrometry (MS) experiments were performed on six cerebrospinal fluid (CSF) and serum samples from four TBI patients. GFAP was immunoprecipitated using a rabbit polyclonal anti-GFAP antibody that was cross-linked to protein G conjugated magnetic beads (Dynabeads) using dimethylpimelimidate-2 (freshly prepared 20mM DMP in 200mM triethanolamine, pH8.6) followed by heat/ice denaturing and reduction in 1% ß-mercaptoethanol [19, 27, 105]. Eluted material was separated by preparative SDS polyacrylamide gel electrophoresis (SDS-PAGE) using 10% NuPAGE gradient gels in morpholinoethansulfonic acid buffer in reducing conditions along with a molecular weight standard (Benchmark). Gels were Sypro-Ruby stained and fixed in 10% methanol, 7% acetic acid. GFAP bands were cut out under UV light and placed into tubes for in-gel trypsin digestion. A fraction (~1/9th) of the eluate was blotted and GFAP was detected using a mouse monoclonal antibodies (mabs) to GFAP (mab1A64-244, Abbott Diagnostics or mab 3E10, EnCor Biotechnology Inc., Supplement Table S3) to provide reference signals for gel band excision. Bands at 50 and 25kDa were omitted to avoid immunoglobulins (Supplement Fig. S1). Gel bands were fully destained, dried, and then reduced with 10mM tris(2-carboxyethyl) phosphine in 100mM ammonium bicarbonate buffer at 56°C for 30min followed by alkylation with 100 mM iodoacetamide in the same buffer at 37°C for 15min. The bands were equilibrated with acetonitrile (ACN), dried, and digested using 0.01mg/ml sequencing grade trypsin in 100mM ammonium bicarbonate buffer at 37°C for 12h. Peptides were extracted from the gel bands by three rinses of 50% ACN/0.1% formic acid solution at 37°C for 15min and the combined extracts were dried in a vacuum concentrator. The peptides were measured by liquid chromatography-tandem MS (LC-MS/MS) using an Ultimate 3000 nano-LC instrument (1h gradient) coupled to a Q-Exactive Plus Orbitrap mass spectrometer. Full spectra (MS1) were collected at a resolution of 70,000 and the 15 most abundant ions of each scan were subsequently fragmented by higher-energy collisional dissociation (HCD; MS2) with a resolution of 17,500 and a dynamic exclusion of 45s. Digestion of defined amounts of recombinant human GFAP served as technical controls (Supplement Figure S2). MS data were searched against the human GFAP protein sequence (Uniprot (https://www.uniprot.org/uniprotkb/P14136/entry) via Proteome Discoverer (PD) version 1.4. SEQUEST-engine confirmed peptides were unique to GFAP (not shared by e.g. vimentin, neurofilaments). "High" confidence peptides (green on maps) had at least two peptides filtered using ≤1% false discovery rate (FDR) threshold of cross-correlation "X-corr scores" for peptide matches contingent on ion precursor charge states. Few "medium" confident peptides (yellow) had at least two peptides with ≤5% FDR (Fig. 1; Supplement Table S8). Identified PTMs included acetylation and citrullination that were further validated by: (a) a unique

signatures of citrullination (immonium ion at m/z 130.0975 and/or neutral loss of isocyanic acid at 43.0058Da) or lysine (K) acetylation (cyclized immonium ion at m/z 126); (b) a MS2 product of b- and y-ions documented mass increments consistent with modifications (Supplement Fig. S10); (c) a comparison of identified citrullination sites after treatment with peptidylarginine deiminase (PAD) enzyme [65].

Partial chemical cleavage of GFAP for monoclonal antibody epitope mapping

The binding region of mab anti-GFAP clone 5C10 was determined initially by binding to the peptide covering amino acids (aa) 233-261 of the human coil2A sequence using dot blots (AALKEIRTQYEAMASSNMHEAEEWYRSKF). The specific epitope was subsequently identified using partial chemical cleavage at tryptophan, which there is only one in GFAP, aa W256. Recombinant GFAP (33µg) was treated in excess with 1% BNPS-Skatole (100µg; 1mg/ml glacial acetic acid; 3-bromo-3-methyl-2-(o-nitrophenylsulfenyl)indolenine, Sigma, Supplement Fig. S11), an oxidant and brominating agent selectively cleaving proteins at tryptophan residues [55, 152]. An equal volume of distilled water precipitated BNPS-Skatole that was removed by centrifugation (5min at 12,000rpm). The supernatant was lyophilized and the GFAP and tryptophan-cleaved BDPs were separated by SDS-PAGE, blotted followed by mab incubation of 5C10 or 3E10, a coil1 GFAP antibody, and a pan-intermediate filament antibody, IFA (hybridoma supernatant, epitope coil2B aa 358-377: ALDIEIATYRKLLEGEENRI) [77, 128].

Western blotting using scaled densitometry and GFAP calibration

SDS-PAGE was conducted as previously described using 7.5% acrylamide for αII-spectrin, 12% gels for GFAP [54]. Protease inhibitors (cocktail CompleteMini, Roche 1:50) and EDTA (10mM) were added to TBI patient CSF, samples were equilibrated to Laemmli sample buffer, boiled for 5min followed by ice incubation and ß-mercaptoethanol to 1% was added prior to loading 34 µl/lane. The same procedure was followed for astrocyte lysates and concentrated culture media described below. Samples and molecular weight standards (Kaleidoscope, Biorad) were collected upon initial run for 30min at 100V and separated for 1h at 120V until the bromophenol blue front reached the bottom. Proteins were cold transferred at 120V for 3h onto nitrocellulose and stained with Ponceau S. Membranes were blocked in 10% non-fat milk in Tris-buffered saline with Tween (TBST) at room temperature (RT) prior to incubation with primary antibody in 5% BSA in TBST overnight at 4°C. Secondary antibodies conjugated with peroxidase (Pierce) were incubated in 5% BSA in TBST for 1h at RT. Enhanced Chemiluminescence (ECL) substrate was applied to washed membranes for 5min at RT (Pico and Femto ECL, Pierce) and multiple exposures were used either of Kodak films or with an iBright imager (ThermoFisher Scientific). Calibrants were recombinant human full-length GFAP and a 20kDa His-tagged GFAP-BDP (aa 72-217, EnCor Biotechnology Inc.) diluted with 0.5% BSA in TBS at defined concentrations (0.08-2.6ng) that were measured at different exposures (Supplement Fig. S5, Table S4). Densitometry was performed on eight exposures from each blot (2s-20min) after background correction. Subsaturated band measurements were standardized to 1min by multiplying shorter exposures and by dividing longer exposures using scaling factors between exposures that were empirically determined from same unsaturated between two exposures (Supplement Table S4). Band sizes were computed using distances of each molecular weight marker from the gel-front and curve-fit equations.

Antibodies used on TBI CSF and astrocyte samples

All antibodies are tabulated with known epitopes, sources, dilutions and Research Resource Identifiers (RRIDs, Supplement Table S3). A rabbit polyclonal GFAP antibody (DAKO) was used for immunoprecipitation and immunoblotting. For densitometry the antibody was applied initially at a high dilution (1:20,000-150,000) for detecting full-size GFAP and large GFAP-BDPs, followed by a lower dilution (1:5,000-7,000) for detecting small GFAP-BDPs, which were adjusted in subsequent scaling. Mab 3E10 was generated to a recombinant construct containing aa 72-217 of human GFAP, comprising coil1A and 1B. The epitope for 3E10 was localized to aa 196-210 (EIRFLRKIHEEEVRE), using peptide competition with a set of

20 nested aa peptides, each overlapping by 5aa. Additional mabs were 5C10 (EnCor Biotechnology Inc.), 1A64-244 (Abbott Diagnostics), a mixture of three clones (4A11, 1B4, 2E1, BD Pharmingen) and mab GA5 (Sigma [26, 28]). Citrullination studies used clone CTGF-1221 that was kindly provided by Akihito Ishigami (Professor, Tokyo Metropolitan Institute for Geriatrics and Gerontology) to detect citrullinated GFAP (cit-GFAP) at aa sites R270 and R416 [61]. Anti-peptidyl-citrulline antibody clone F95 (EMD Millipore) validated citrullinations. Several additional rabbit polyclonal citrullination site-specific GFAP antibodies, including cit-GFAP-270, were generated and characterized (BRAINBox Solutions, Inc.). A mab against αII-spectrin was used at 1:3,000-1:5,000 dilution (Enzo Life Sciences).

Human cerebral astrocyte trauma model

Human culture trauma model: In vitro differentiated fetal cerebral astrocytes were prepared as previously described [155]. Briefly, cortical tissue was mechanically dissociated, filtered and astrocytes were enriched by Percoll gradient centrifugation. Cells were expanded in DMEM/F12 with 10% fetal bovine serum. Residual oligodendrocytes and progenitor cells were removed by shaking. Astrocytes were seeded on collagen-I coated deformable silastic membranes at 138,000-180,000 cells/9.62cm^2 and differentiated in DMEM/F12: Brainphysiology Medium supplemented with SM1 and N2A (Stem Cell Technologies) by stepwise serum removal. Astrocytes were traumatized by 50ms pressure pulses (4.9-5.3psi) that abruptly stretched the culture bottom, shearing the cells compromising membrane integrity that led to delayed cell death [54].

Live microscopy imaging: Cerebral fetal human brain cells were differentiated for three weeks by serum withdrawal in a 1:1 mixture of DMEM/F12: Brainphysiology medium (StemCell Technology). Live imaging was done 5h after stretch injury on a Leica DMI8 microscope in a gas and temperature-controlled chamber (Okolab). Cells were bathed for 5min in 60µM propidium iodide (PI, Sigma) to label leaky membranes. Washed cultures were live-imaged in the presence of two permeable fluorescent protease substrate reporters for calpains (30µM CMAC tBoc Leucyl-methionine, ThermoFisher), and for caspases (5µM DEVD-NucView488, Biotium).

Astrocyte protein sample preparation for gel electrophoresis: Whole cell lysate (WCL) of adherent astrocytes was prepared by adding 150µl lysis buffer/9.62 cm^2 wells (150mM NaCl, 20mM Tris, 5mM EDTA, 10mM NaPyrophosphate, 30mM phosphatase substrate, 5mM dithiothreitol, DTT (Calbiochem)), 1% NP40 and 1 tablet/10ml protease inhibitors (Mini Protease Inhibitor Cocktail, Roche). Lysis buffer was incubated for 5min at 4°C, lysates were collected by scraping into low binding tubes and homogenized by 3x5s sonification bursts without foaming (Branson Digital Sonifier, 90% or constant amplitude duty cycle, output level 5). Culture medium conditioned by astrocytes (CM) without serum or protein supplements was collected and 5mM DTT and 1tablet protease inhibitors /10ml added. Particles from lifted cells and debris were pelleted by initial centrifugation (5000g, 5min, 4°C) and then lysed for 5-10min in 0.5% lysis buffer followed by 3x5s sonication. Remaining insoluble fractions were removed by centrifugation (10min at 16,000g 4°C). Media were concentrated (Vivaspin, 3kDa cutoff) by centrifugation (4-8h at 5000g, 4°C) to ~1/10th-20th of the original volume to obtain a protein concentration of 1-1.5 µg/ml. All samples were immediately frozen in aliquots at -80°C.

Protease inhibition in the human trauma culture model: Pan-calpain inhibitor calpeptin (13µM Z-Leu-nLeu-H, Millipore/Sigma), a non-toxic cell-permeable peptide aldehyde inhibitor [83, 167]. Pan caspase inhibitor ZVAD-FMK (11µM benzyloxycarbonyl-Val-Ala-Asp(OMe)-fluoromethylketone; Enzo; ThermoFisher) is a cell-permeable, irreversible pan-caspase inhibitor that is effective against a spectrum of caspases (1-10, except 2; Invitrogen) [40]. ZVAD-FMK is reported showing also calpain inhibition after controlled cortical impact to the mouse brain [73]. Inhibitors were applied 10min to cultures after stretching omitting gentamicin in the medium and were incubated with cells for 5, 24 or 48h replenishing drugs every 8-10h. Other tested calpain inhibitors included leupeptin (20µM) and SJA6017 (10µM Calpain Inhibitor VI, Calbiochem) had limited effect, were toxic by either increasing cell permeability as did PD1500606 (100µM,

Calbiochem), or by increasing cell death as did MDL28170 (Z-Val-Phe-al, 4μM, Calbiochem) and were not further pursued.

Statistical analysis approaches

GFAP band measurements were assessed for normality by the Shapiro Wilk criterion for Gaussian distribution fit. GFAP and GFAP-BDP measurements deviated from normal distribution, determined by significantly lowered W-values, and were log-transformed replacing zero with half of the lower limit of detection (0.7pg or a concentration of 27pg/ml; Supplement Fig. S6).

***Reproducibility*:** Immunoblot densitometry reproducibility was determined on technical replicates using the coefficients of variation (CV=SD/mean x100, Supplement Table S5).

Covariates: Effect modifiers patient age, race, sex and concurrent body temperature, and their interactions were evaluated.

Model of variance components: Used was a restricted maximum likelihood (REML) linear mixed model (LMM) with patient identifiers (IDs) as random effect to account for repeated measures per patient. Added to the model was injury elapsed days, and knotted spline estimation.

Effect testing: For the effect of age, partial omega squared (ω_p^2) was used to report the proportion of the population variance fixed effects because it adjusts for variable sample size [78]. It was computed using fixed effect statistic (F-statistic) results of the REML-LMM output in SAS/Jmp along with degrees of freedom (df) and its denominator term (DFDen) as follows: (1)

$$\omega_p{}^2 = \mathrm{F} * \mathrm{df}_{\mathrm{effect}} - (\mathrm{df}_{\mathrm{effect}}/\mathrm{F} * \mathrm{df}_{\mathrm{effect}}) + \mathrm{DFDen} + \mathrm{df}_{\mathrm{effect}}.$$ (1) *Age covariate effect formula*

Temporal profiles: Longitudinal means were graphed by spline fit lines from resampled daily CSF draws along with 95% confidence intervals (CI, Figs. 7C, 8). Temporal GFAP and fragment trajectories were evaluated using REML-LMM with age as covariate (Supplement Table S7 and Figure S13). Cohen's D effect sizes on each postinjury day (PID) were computed using adjusted means (Adj.Means) on each PID compared with overall means weighted for sample availability on each day [59, 110] with pooled (SD) from the total random variance component (Supplement Table S8, Supplement Figure S10) [80]. Formula (2):

$$\mathrm{Cohen's\ D}_{\mathrm{forGRAP\ by\ PID}} = (\mathrm{Adj.\ Mean}_{\mathrm{PID}} - \mathrm{Adj.\ Mean}_{\mathrm{Overall}})/\sqrt{pooled}\ SD$$ (2) *Time effect formula*

Bivariate correlations: To assess GFAP substrate-product and product-product relationships, log-transformed GFAP band signals were pairwise correlated reporting uncorrected Pearson correlation coefficients (Fig.3, Supplement Fig. S8). Biplots used orthogonal fit for equal variance between GFAP bands and are reported with coefficient of determination (R^2) and Benjamini-Hochberg-based FDR-corrected Logworth, [-$\log_{10}$(p-values)], (Fig. 3). The outlier portion is documented with robust correction defined as percent of datapoints with a distance exceeding 3X the residual SD. Correlation outliers that might affect the correlations across all variables were inspected using the Mahalanobis distance to determine potential multivariate outlier with the threshold being the upper control limit, UCL and calculated using sample size and the number of variables used, by applying robust weighting to discern outliers [52, 81, 149].

Outcome prognosis: The GOSE score was used to assess six-month recovery prediction by longitudinal GFAP profiles. GFAP trajectories are shown for good (GOSE 5-8), and poor (GOSE 1-4) outcomes and were graphed using cubic splines with same curvature fit (λ= 0.28) and 95% CI (Fig. 4). GFAP profiles were assessed for their ability to distinguish good versus poor outcomes using a REML-LMM model with ID as a random and elapsed PIDs (modeled with knotted splines) as a fixed effect and controlling for age. Differences in GFAP adjusted means between good and poor recovery were calculated as described as follows in formula (3).

$$\text{Cohen's D}_{\text{for outcome}} = (\text{Adj. Mean}_{\text{GOSE poor}} - \text{Adj. Mean}_{\text{GOSE good}})/\sqrt{pooled\ SD} \quad (3)$$

Outcome effect formula

Cohen's D in SD units here uses total residual variant component capturing within-subject variability (Supplement Table S7). Fig. 3D shows adjusted means using above REML-LMM model with standard errors and post-hoc t-statistic and patient ID as random effect and elapsed postinjury time as fixed effect.

Label-free MS analysis: A) Peptide presence/absence frequency was compared between coil1 and coil2 peptides using a mixed model with unequal variances, patient ID as random and GFAP-BDP sets as fixed effects. B) The peak ion abundance of coil1 versus coil2 ions was compared using a mixed model analysis with ID as random and GFAP-BDPs as fixed effect while undetected peptides were excluded (Fig. 1D; Supplement Fig. S3).

RESULTS

Novel trauma-specific GFAP breakdown products in TBI patients and their fluid imbalance

GFAP-BDPs in TBI patients differ from Alzheimers and Alexander Disease fragments

GFAP displays a range of fragments and cytoskeleton proteolysis is increased after TBI [34, 54]. Here, we determined TBI-specific GFAP degradation by sequencing fragments of immunopurified gel-slices (I.-IV.) using MS in six TBI CSF samples (Supplement, Fig.S1). Molecular masses of each size-range were estimated pooling slice-specific high-confidence peptides from each patient and compared with band migration on GFAP immunoblots (Fig.1AB). Bands (I.) contained a 41.7kDa fragment. Bands (II.) migrated between 36-39kDa as shown in GFAP immunoblots and contained peptides covering a calculated mass of 40.6kDa. This slightly higher mass from pooling indicates variable proteolysis across patient's samples. Further, charged GFAP residues may have contributed to slightly faster gel migration [49, 138]. Bands (III.) contained two BDPs of the alpha-helical rod domain: a coil1 covering 21.8kDa product and a 17.5kDa coil2B product (Fig.1AC). Bands (IV.) included a shorter coil1-BDP (21.3kDa) and a shorter coil2-BDP (15.2kDa). These sequences confirm previously observed 42, 37 and 18-25kDa GFAP-BDP bands and support a consecutive cleavage producing various sized coil1 and coil2 products [54]. None of the small products covered peptides in coil2A, the linker region between them, while these aa were readily detected in larger bands (47, 50kDa) and in full-length recombinant GFAP (Supplement Fig.S2). Peptide absence between the two coil products suggests one or more previously uncharacterized trauma-specific cleavage site(s), which was further investigated in a human trauma model (see below).

Coil1 products had the same N-terminus yet a four-residue larger C-terminus in slice (III.) versus (IV.) These coil1 products extended beyond a prior reported caspase 6 cleavage (at VELD225) associated with Alexander disease [26]. Immunoblots using a polyclonal antibody detected small GFAP-BDPs within these observed molecular masses (Fig.1C). Coil2-products had the same N-terminal phenylalanine (F261) but distinct C-termini, with the longer one ending at K410 (151aa, 17.5kDa in slice III.) and the shorter coil2 ending at arginine (R390, 130aa, 15.2kDA, in slice IV., Fig.1AB). Coli1 mab 3E10 did not detect the 17kDa band confirming its coil2 (Fig.1B, Supplement Fig.S1). Notably, the TBI-associated 15-17.5kDa coil2-products were consistent with an AD-reported caspase 3 cleavage site (aa residues 258-266, RSKFA↓DLTD), but smaller than the 30kDa GFAP fragment identified in Alzheimer's disease (AD) samples [106]. Documenting different GFAP-BDP endings in TBI versus other neurodegenerative diseases underlines

conditional specificity in its proteolysis and hence limits extrapolation from recombinant GFAP digests in cell-free systems or after toxin treatments [166].

Imbalance of coil1 and coil2 GFAP breakdown products in TBI patients' biofluids.

As high-confidence green peptide markings show, coil1 had greater coverage than coil2 products. This imbalance was quantified showing peptide frequencies across MS runs with significantly higher coil1 (59±29%) versus coil2 (13±7%) frequencies (Fig.1D). Ion peaks were significantly higher in coil1 over coil2 peptides, further supporting greater coil1 abundance in TBI CSF (Supplement Fig.S2). In serum, TBI had elevated 37kDa and 20kDa bands over control (Supplement Fig.S4A). Immunoprecipitated GFAP from four different TBI serum samples of two patients identified a coil1-product spanning aa51 to R217 (97 residues, 18.2kDa, Supplement Fig.S4). With 59% sequence coverage, the termini could not be confidently identified. Noteworthy, coil2-containing peptides were absent, further underlining a TBI biofluid imbalance between the two coils.

In summary, deep sequencing of GFAP-BDPs in TBI patient biofluids identified proteolytic processing expected to generate equimolar coproducts, yet coil1-products were overrepresented over coil2 products. Prevalence of these GFAP-BDPs was further validated in a cohort TBI patients' CSF.

Temporal GFAP proteolysis and fragment-specific imbalance in neurointensive care TBI patients

Temporal dynamic of GFAP degradation after TBI

MS fragment sequences were validated by independently quantifying matching GFAP bandsets in 23 TBI patients' serial CSF samples over ten postinjury days (PIDs). Scaled immunoblot densitometry allowed standardizing multiple sub-saturated exposures followed by calibration to known dilutions of intact and small BDP recombinant GFAP proteins. This expanded the dynamic range to span four-five orders of magnitude documented by limits of detection and quantification (Supplement Table S4, S5, Fig.S5). Inter-experimental replicates provided technical reproducibility with average CV of 27.8% (Supplement Table S5) [78].

Longitudinal GFAP profiles document substantial variability in summated GFAP ("Total"), full-length and degradation products over ten PIDs across patients expressed by interquartile range (IQR), kurtosis and variance (σ) for each bandset (Fig.2). GFAP levels increased significantly with patient age, as it contributed 23-38% to the residual variance of uncleaved GFAP and three sets of GFAP-BDPs after adjusting for time and donor effects (ω_p^2, Supplement Table S6, Fig.S7). Total GFAP levels peaked on injury day with age-adjusted effect size of 1.3 SD units above the weighted mean (Cohen's D, p=0.035, Figure 2C). Most bands' daily means exceeded the overall mean on until PID4, and by PID7 onwards means were observed below overall mean documenting an overall GFAP decline in CSF over time. Specifically, mean profiles of uncleaved and large 45-49kDa fragments declined significantly over time, while all other fragments (15-39kDa) had also secondary raises (Fig.2F-H). This distinction supports ongoing proteolysis contributed to the longitudinal GFAP pattern. The two sets of small GFAP-BDPs had wider confidence bands caused by secondary peaks along many undetectable values, prompting further inspection.

Fragment covariation and imbalance of small GFAP-BDPs

Strongest correlation was determined between 50kDa GFAP and 37-39kDa fragments (Pearson coefficient, r=0.82, R^2=0.68, LogWorth=24.3; Fig.3). The 40-42kDa fragments correlated similarly with the 37-39kDa fragments (r=0.73, LogWorth=16.3). These plausibly reflect co-release of substrates and intermediary products. Small BDPs, notably the 15-19kDa bandset had weaker relationships with precursors (Fig.3; Supplement Fig.S8). Further, 15–19kDa BDPs had 28% more undetected values than 20–26kDa BDPs across patients (Fig.3C). Small BDP coproducts covaried also less with one another. This TBI cohort quantification provides further evidence for a selective absence imbalance among small GFAP products supporting MS-observed coil1/2 imbalance. These findings are further explored using a trauma culture model for mechanistic insight (see below). Given both full-size and fragment GFAP species in our dataset, we sought

to determine which GFAP proteoforms would result in better outcome prognosis in moderate-severe TBI [132]. This distinction may inform whether uncleaved GFAP or its post-traumatic proteolysis relate better to overall TBI recovery.

Profiles of GFAP fragments predict TBI outcome but not that of full-length GFAP

To investigate how GFAP degradation relates to patient recovery after TBI, we compared longitudinal CSF levels of full-length GFAP and its fragments in patients with favorable versus unfavorable six-month outcomes using GOSE. Age-controlled CSF means of 37-39kDa GFAP-BDPs distinguished patients with poor outcome (GOSE 1-4) from those with favorable outcome (GOSE 5-8, Cohen's D: 1.1 Standard deviational units, p=0.02; Fig.4A, Supplement Table S7). Small 20-26kDa BDPs separated good-versus-poor GOSE early postinjury with lower levels in patients with good outcome, while adjusted means overlapped during later PIDs (Fig.4B). Same GOSE-binarized partitioning of full-length GFAP signals led to substantial mean and confidence band overlap between poor and good recovery across ten PIDs. Similar outcome prognosis for same GFAP proteoforms were observed using stricter partitioning of favorable outcome (GOSE7+8), indicating the findings were independent of the way GOSE scores were dichotomized (Supplement Fig.S9). In summary, longitudinal profiling of GFAP degradation products informs on temporal proteolysis and provides greater prognostic resolution than full-length GFAP.

Citrullinated GFAP-BDPs show a TBI patient signature distinct from that of classic GFAP

The uneven fluid presence of stoichiometrically equimolar generated coproducts was measured by label-free MS comparison of coil1 and coil2 peptide abundances and by immunoblot densitometry of small GFAP-BDPs supporting selective coil2 fluid deficits. We then investigated whether TBI-associated GFAP modifications may be present in CSF possibly associated with fragment disparity. Acetylation and citrullination promote selective destabilization and aggregation and associate with neurodegeneration [23, 67, 82, 101, 154]. Notably, citrullination has a destabilizing effect on intermediate filaments, is reported in rodent injury models and citrullinated GFAP is observed in chemically stressed cell lines and cell-free systems [62, 65, 82, 124, 161]. To our present knowledge, GFAP-PTMs have not been characterized in human TBI patient samples.

Validated mapping of citrullination and acetylation in GFAP fragments from TBI patients

We analyzed mass spectra of coil1/2 GFAP-BDPs for acetylation and citrullination to identify PTM signatures in TBI, to support biomarker assay development and to detect cytoskeleton-destabilizing events and proteinopathies. MS-detected acetylated and citrullinated peptide fragments were validated through presence of signature ions and neutral mass losses (Supplement Table S8). Three lysine acetylations were validated in coil1, and four citrullinated arginines in coil1, including a potential novel citrullination site in coil1 (R79), and three citrullines in coil2, which were all consistent with observed mass deviations in MS2 spectra (Fig.5A, Supplement Fig.S10, Table S8). Additional five citrullinations detected in this TBI CSF samples set is validated reported as in vitro modifiable GFAP sites citrullinated by PAD treatment [65]. These GFAP-BDP acetylations and citrullinations in TBI-CSF were robust, as they were repeatedly detected.

TBI patients have different citrullinated GFAP signatures

Citrullination was further analyzed using site-specific citrullinated GFAP antibodies (Supplement Table S3, epitopes see Fig.5A) [61]. Two cit-GFAP antibodies with neoepitopes in coil2 gave patient-specific signals distinct from those of classic GFAP (Fig.5B). Cit-GFAP signals strongly detected 13-16kDa and 26-30kDa GFAP-BDPs compared to larger proteoforms and clearly distinct from the band signal proportions of unmodified GFAP detected in same samples (Fig.5B right). Large GFAP-BDPs were detected by CTGF-1221, as it is reported with a second epitope (R416) to the more c-terminal region located outside of coil2, whereas cit270-GFAP is directed solely to R270 within coil2. Additional citrullinated bands above 50kDa are likely

pathological GFAP proteoforms, possibly ubiquitinated or multimeric forms [113, 161]. Notably, these patterns had substantial patient-to-patient variation that highlight individual differences in proteolysis and PAD activities during TBI progression. These preliminary observations support an interest in including modified GFAP for future TBI patient molecular profiling.

To further investigate trauma-induced GFAP proteolysis and the disparity between coproducts, citrullination, and their association with injured astrocytes, we employed a human culture trauma model for mechanistic insights.

Mechanistic exploring of GFAP proteolysis and modification in a human astrocyte trauma model

A series of epitope-defined GFAP antibodies was used to map coil1 and coil2 products for tracking their destiny and defining GFAP cleavage site after trauma. Inhibitors and reporters then documented calpain and caspase contribution to traumatic GFAP degradation and activity in injured human astrocytes. Lastly, citrullinated GFAP aggregates identified pathological astrocytes providing an explanation for selective fragment retention.

Trauma-generated GFAP coproducts are destined to different locations

Primary fetal human cerebral astrocytes were in vitro differentiated on elastic membranes and were reproducibly injured by abrupt pressure-pulse stretching [155]. GFAP filaments are disassembled, degraded and released in this trauma model [54]. To identify coil-specific BDPs, mabs with defined GFAP epitopes were probed on immunoblots of WCL (“cells”) and concentrated CM (“fluid”) of unstretched controls and stretched cultures from the same donors (Fig.6, Supplement Table S3). All clones detected full-length GFAP and large fragments but differed in small BDPs [70]. Clone 3E10 detected a 20kDa GFAP-BDP in astrocyte CM that increased after trauma, yet failed to detect it in cells (Fig.2C, red). Clone GA5 detected an epitope at the end of coil2, beginning of the GFAP tail [28]. GA5 detected a set of 17-28kDa GFAP-BDPs in cells but not in fluids (Fig.2C, purple). A cocktail of three mabs served as positive control, proofing GFAP-BDPs in cells and fluids from same donors (Fig.2C, blue). Thus, following mechanical trauma of human astrocytes, coil1 products were preferentially released, while coil2 products were selectively retained within cells. This new human trauma model insight supports the enriched presence of coil1 BDPs in biofluids of TBI patients.

Mapping a novel GFAP trauma cleavage site

Clone 5C10 detected full size and large GFAP-BDPs in cells and fluids of same donors, but no fragments smaller than 40kDa in either compartment. This suggests that 5C10 recognized an epitope that was destroyed during trauma proteolysis of GFAP (Fig.2C, yellow). To pinpoint the 5C10 epitope, we performed a chemical-mediated partial digest of GFAP using BNPS-skatole that cleaves after tryptophan residues as there is only a single tryptophan in GFAP (W256) [55, 152]. BNPS-skatole treated GFAP produced a N-terminal 34.6kDa and a C-terminal 20.5kDa fragment and 5C10 bound avidly to the C-terminal fragment on western blots (Supplement Fig.S10). The identity of the C-terminal 20.5kDa BNPS-skatole fragment was confirmed using anti-IFA, a pan-intermediate filament antibody to coil2B [77, 128]. 3E10 coil1 antibody bound the N-terminal 34.6kDa BNPS-skatole fragment not detecting the C-terminal BNPS-skatole fragment. This concludes that the sequence following tryptophan W256 from tyrosine 257 to tyrosine 260 (aa YRSKF) is an important component of the 5C10 epitope. As 5C10 does not detect small GFAP-BDPs after trauma, this also informs of the trauma-induced cleavage site in this region. It may likely include elements of the neighboring caspase 3 cleavage site, (aa YRSKFA↓DLTD). By MS identified TBI-patient detected coil1 sequence extended no further than R239 and the beginning of coil2 products were consistently observed F261 pinning the cleavage within this area. This unique antibody mapping data identified a novel trauma-cleavage upstream of F261 combined with potential caspase 3 activity downstream of it (Fig.6AB).

To determine the in rodents characterized contribution of TBI activated calpains and caspases in producing small GFAP-BDPs, we used suitable inhibitors and live-imaging reporters in the human trauma model [11, 34, 74].

Generation of small GFAP-BDPs involves calpains and caspases

Human traumatized astrocytes were treated with calpain inhibitor calpeptin (C), or caspase inhibitor ZVAD-FMK (V), and GFAP-BDPs were analyzed in WCL from adherend cells, fluids, and pelleted lifted cells and debris. αII-spectrin with its calpain and caspase-defined fragments (SBDPs[139, 151]) served as positive control, as they were expressed in differentiated human fetal astrocytes (Supplement Fig. S11) as reported in human astrocytes [72]. Both calpain (145/150kDa) and caspase (120kDa) SBDPs increased two days after stretch-injury in cells, debris, and fluids and decreased with respective inhibitors (Supplement Fig.S6). The 120kDa caspase-SBDP was enriched in detached material of demised cells. Note, both calpain-SBDPs were observed as double-band in WCL, yet a single 150kDa band was found in lifted cells, and a single 145kDa band was detected in fluid. These findings suggest that αII-spectrin calpain fragments originated intracellularly and had distinct compartment preferences after trauma alike what we found for GFAP-BDPs.

Two days post-stretching, GFAP-BDPs were elevated in cells, fluid and lifted material (Fig.7A, Supplement Fig.S12A). Calpeptin reduced 35-38kDa and smaller BDP bands. ZVAD-FMK effectively inhibited 19-26kDa BDPs. Combined inhibitors had an additive effect, confirming that both calpains and caspases were involved in human GFAP degradation after trauma. GFAP-BDPs were present in smaller amounts in unstretched samples, also inhibitor-sensitive, consistent with baseline cytoskeleton turnover [124]. Undigested GFAP initially (5h postinjury) accumulated in the cytoskeletal-soluble WCL samples (Supplement Fig.12B). At two days with calpeptin inhibition 50kDa GFAP increased in WCL of cells and lifted material indicating accumulated substrate (Fig.7A, Supplement Fig.12C). This suggests filament disassembly as an early trauma consequence followed by calpains digesting GFAP monomers. This data provides the first evidence of endogenous trauma-inflicted calpain and caspase digestion of human GFAP going beyond prior rodent work [166].

Given the limited knowledge of human astrocyte injury states relative to the expanding literature on GFAP as TBI biomarker, we next used live protease activity reporters combined with a membrane integrity dye and fixed citrullinated GFAP immunofluorescence to characterize astrocyte injury phenotypes. These microscopy pathophysiology studies aim to further characterize human traumatized astrocytes in our trauma model that previously linked GFAP fluid elevation to percent cell wounding [54].

Acute astrocyte injury states related to membrane wounding and proteolysis

Human astrocyte pathophysiology after stretch-injury is shown using live-fluorescent calpain and caspase reporters together with PI to assess membrane permeability. These differentiated human astrocytes displayed two morphotypes, fibrous elongated cells and bushy, star-shaped cells, resembling white and gray matter astrocyte morphologies [3] (Fig.7B). Under control conditions, both types showed calpain but rarely caspase activity, consistent with fetal neocortical expression of calpains along with low calpastatin [136]. Five hours post-stretching cultures showed a mix of astrocytes with leaky and intact plasma membranes documenting dynamic membrane damage. Injured fibrous astrocytes lacked calpain activity and frequently displayed beaded, clasmatodendrotic processes with caspase activity (Fig.7BC) [31, 54]. Injured bushy astrocytes were simultaneous calpain and caspase activ, lost radiating processes and had blebbing with phase-dark vesicles and vacuoles devoid of enzyme activity (Supplement Fig.S13). Acutely pyknotic cells, defined by shrunken phase-dense morphology, had bright PI-stained nuclei and either no active protease, or active caspases, indicating progression towards integrity loss, early necrosis or a transition from apoptosis to secondary necrosis. Thus, we identified a novel pathological phenotype of acute degenerating dystrophic human astrocytes exhibiting both active protease activity and membrane wounding hours after trauma.

These initial images document concurrent injury phenotypes and proteolysis states in human traumatized astrocytes illustrating a spectrum of early vulnerability. This model offers an opportunity for future temporal proteolysis analyses and associated aberrant proteoforms. For this initial study, we examined GFAP proteoforms by coil2-specific antibodies in traumatized astrocytes.

Citrullinated GFAP in traumatized astrocytes detects pathological aggregates

Distinguishing GFAP proteoforms in traumatized astrocytes is critical, as typically the prominent reactive astrogliosis dominates astrocyte documentation after insults. As our findings thus far indicate, coil2-GFAP-BDPs preferred cellular residence, hence we chose two coil2-specific antibodies, cit270-GFAP detecting citrullinated coil2 and 5C10 to coil2/tail of classic GFAP alongside a polyclonal GFAP antibody for comparison after confirming specificity of cit270-GFAP signals (Supplement Fig.S14A). Stretch-trauma cultures had visibly more cit270-GFAP signals than controls at 5 and 24h postinjury (Fig.8). Cit270 stained clusters, speckles and large granules but did not stain cytoskeletal fibers as shown by staining for unmodified GFAP. Cit-GFAP aggregates and GFAP filaments showed distinct distributions. Cit-GFAP stained either cells negative for classic GFAP, or excessively bright stained cells. Increased GFAP antigenicity is reportedly associated with filament disassembled GFAP after acute wounding, calcium ionophore-treatment, or calpain activation in astrocytes [54, 84]. Morphotypes with cit-GFAP granules included reactive, shrunken or swollen dystrophic astrocytes devoid of processes (Fig.8B, Supplement Fig.S14D). Cit270 signals were also peppered around astrocyte processes seemingly extracellular, as phase-contrast images delineated astrocyte shapes (Fig.8B, Supplement Fig. S14E). Thus, mechanical injury-induced GFAP citrullination and filament breakdown identified pathological astrocytes hosting dysfunctional GFAP. This finding provides evidence for coil2-associated aggregation that could contribute to its selective cellular retention and underrepresentation in TBI patients biofluids. It further establishes cit270-GFAP as a proteinopathy marker of pathological GFAP aggregation associated with human traumatized astrocytes and new tool to study astrocyte degeneration relevant to the pathophysiology of TBI.

In conclusion, TBI patients show GFAP destabilization by citrullination and acetylation, and trauma-specific proteolysis, producing unique small coproducts with distinct release behaviors. The observed coil-specific BDP fluid imbalance in fluids is driven by citrullination-modified GFAP aggregation, highlighting a GFAP proteinopathy in pathological astrocytes. Notably, CSF trajectories of GFAP proteolysis, not the uncleaved protein release, predict outcome, underscoring the diagnostic value of monitoring postinjury processes including proteostasis disruption for TBI patient evaluation.

DISCUSSION

This study identifies novel TBI-specific GFAP proteolysis as a dynamic process generating proteoforms with distinct patient-specific longitudinal trajectories. The trauma-derived small GFAP-BDPs directly document an association between previously in neurotrauma unrecognized proteinopathy in pathological astrocytes with GFAP as biofluid marker. These results suggest that disrupted proteostasis may contribute to the underlying TBI pathophysiology and could play a role in shaping patient recovery, warranting further studies beyond the conventional view of GFAP as TBI biomarker.

Acute trauma pathophysiology explains early GFAP vulnerability in injured astrocytes

Mechanical trauma, e.g. whiplash or blunt impact, shears brain microstructures causing diffuse axonal injury and astroglial clasmatodendrosis -membrane wounding that can lead to protracted cell loss [31, 42, 54, 141]. This mechanoporation of plasma membranes triggers rapid release of full-length GFAP and its fragments [7, 54, 86]. High-speed biomechanical force or strain can stretch intermediate filaments to disassemble or even break strands thereby exposing the rod-domain making it susceptible to proteolysis [16, 39, 124, 133]. Non-

filamentous GFAP is documented minutes after stretch-injury in mechanoporated human astrocytes [54]. Thus, filament-disassembly is closely linked to membrane permeability that disturbs ion balance and threatens astrocyte viability [54]. Ion imbalance is followed by water influx causing membrane blebbing and astrocyte oncosis (swelling) [24, 50]. With progressive energy depletion, cell integrity may fail resulting in early necrosis. Added stressors such as reactive oxygen species, acidosis and hypoxia further impair mitochondrial function ultimately shift cell death pathways from apoptosis to necrosis [5, 18, 29, 50, 92, 97]. These processes may contribute to secondary GFAP release in TBI patients reflecting cytotoxic edema and delayed astrocyte loss [21, 87, 151, 153, 157, 172].

Citrullination and proteolysis relate to GFAP proteinopathy and impaired astrocyte function

Assembled GFAP filaments are essential for astrocyte morphology, mechanical resilience, ATP release and other key functions [124]. Calcium ionophores induce a rapid, transient increase in GFAP immunocytochemical signals in rat astrocytes due to filament unwinding and epitope exposure [84]. Trauma-induced unfolding and associated calcium influx could similarly expose a concealed proteolytic cleavage site within the GFAP rod. Calcium elevation catalyzes GFAP proteolysis by rapidly activating calpains through conformation change leading to partial GFAP cleavage, consistent with their limited proteolytic activity [7, 22, 30, 33, 36, 69, 84, 91, 104, 124, 125, 156]. Calpain cleavage also primes caspase activity hence both enzymes generate small GFAP-BDPs [45, 91]. Baseline calpain activity is reported as part of the ubiquitin-proteasome, autophagy-lysosomes, and cytoskeleton-remodeling systems, modulated by endogenous calpastatin, consistent with observing active calpain in unstretched astrocytes [48, 127, 136, 139].

Stretching causes focal mechanical loading, producing a range of astroglial injury states that varies further by differences between gray- and white-matter morphotypes as could be indicated by distinct calpain and caspase activities after trauma. Caspase activity in process-damaged astrocytes parallel clasmatodendrosis in excitotoxic injured rat astrocytes further linking cytoskeleton remodeling and caspase-mediated breakdown with apoptosis [1, 22]. As cytoskeleton integrity is necessary for structural resilience and metabolic competence, GFAP proteolysis may exacerbate astrocyte vulnerability as is the case in reduced GFAP expression after injury [86].

Pathological GFAP proteoforms impair astrocyte functions, compromise glutamate buffering and neuronal stability that may exacerbate neurodegeneration [89]. Mechanical stretching, hypoxia and chemical insults induce calcium-dependent PADs destabilize GFAP by elevating its citrullination in astrocytes and Müller glia [4, 135, 161]. Citrullinated GFAP proteoforms are prominently found in Alexander disease where mutant GFAP fragments form toxic aggregates, Rosenthal fibers that contribute to progressive neurodegeneration [26, 28, 35, 53, 89, 101, 130]. Aberrant GFAP critically undermines astrocyte function, neural metabolism, network activity and neurovascular unit integrity [66, 143]. Jointly our observation of trauma-driven cit-GFAP aggregates in pathological astrocytes point to a neurotrauma proteinopathy with potential harmful consequences.

Uniqueness of traumatic injury-produced GFAP breakdown products via coil2A sensitivity

Cleavages that produce TBI-associated GFAP-BDPs are distinct from established protease sites in other neurodegenerative diseases. A caspase 6 GRFAP cleavage ($VELD_{225}$-VAKP) is described in mouse culture models of Alexander disease, splitting GFAP in linker2 [9, 26, 28]. Here we identified longer coil1-products with a TBI-cleavage between residues 240-260. GFAP-BDPs reported in Alzheimer's disease are generated by a caspase 3 cleavage at $_{258}$RSKFA↓DLTD [106]. Our biochemical studies identified ($_{257}$YRSKF$_{261}$) as likely cleavage region flanking this caspase 3 site generating the new N-terminus of the coil2-product, yet coil2 was shorter than the reported AD GFAP-BDPs. The shorter TBI coil1-product end is not explained by this cleavage. Coil2A appears particularly sensitive to proteolysis after TBI and our findings suggest calpains and caspases are involved, though other proteases -including possible endogenous trypsin-like activity could generate the new observed termini (LTAALKEIR↓T; R239). Endogenous trypsin activity is reported after brain injury inflicting astrocyte compromise and adverse inflammatory effects [43, 164]. Joint

proteases can account for the observed sequence gap within coil2A between the two product sets, warranting further studies.

Structural evidence for protease vulnerability of the TBI cleaved region

Intact GFAP molecules anneal by α-helical coiled-coil interactions forming parallel dimers, antiparallel tetramers and ultimately 10nm diameter units that grow in length to mature filaments [70]. Computer modeling and structural data show that the entire rod segment of vimentin, closely related to GFAP, is a continuous α-helix [44]. This is despite several regions, historically referred to as linkers or "stutters", lack the typical hydrophobic heptad repeat pattern of α-helical coiled-coils. These regions contain proline and other turn-promoting aa or feature 11aa (hendecad) sequences disrupting the heptad repeats. These regions are therefore thought to represent non-helical linkers. The Alexander disease-associated GFAP cleavage is found within one such non-helical region, "linker12". Notably, the region containing the MCA5C10 epitope and caspase3 site is historically referred to as "stutter1", where a hydrophobic heptad repeat is replaced by a single hendecad sequence, disrupting the packing and thereby rendering is more susceptible to proteases [145].

Pathophysiological significance and biomarker implications of new GFAP-BDPs

TBI proteolysis of GFAP produces coproducts with unequal abundance in patient biofluids due to differences in release or susceptibility to further degradation -or both. We show preferred coil1- release and selective coil2-BDP retention as non-filamentous cit-GFAP aggregates in traumatized human astrocytes while an in vivo study documents strongly upregulated citrullination in the contused rat brain localized to astrocytes [82]. Thus, cit-GFAP aggregates associate with an astrocyte pathology that we link with GFAP as TBI biomarker.

TBI CSF samples carry both coproducts with coil2-BDPs either absent or elevated. One scenario could involve adverse events that may cause glial integrity loss with release of otherwise retained proteoforms (see below). Astroglial membrane lysis during cytotoxic edema could account for such uncontrolled necrotic or oncotic events (context discussed below) [24, 50]. On one hand, coil1-GFAP fluid may be matched by a latent coil2-GFAP burden in the injured brain. On the other hand, detecting coil2 in fluids may signal worsening conditions such as cytotoxic edema with unregulated astrocyte demise. Thus, coil- and citrullination-specific GFAP antibodies can serve as pathological astrocyte markers and as tools for tailoring assay development in TBI, see below [41, 142, 150]. New possibilities for priorities of future research addressing present needs include to (1) examine cit-GFAP-aggregates in postmortem brains after TBI, BLAST, or chronic traumatic encephalopathy to investigate traumatic astrocytopathy; and to (2) further develop an association of GFAP biomarker, disrupted proteostasis and neurodegeneration [60, 123].

Relevance of GFAP-BDPs for assays design and interpretation

GFAP testing after TBI is already incorporated into large multisite clinical studies for acute patient assessment using commercial antibody-based platforms [12, 13, 75]. However, beyond a general specificity for GFAP it is not clear what proteoforms are being measured, as this information is typically proprietary or unknown and it is presumed that total released GFAP is captured. The distinct release and modifications of coil1 and coil2 products can add insight for design and interpretation of GFAP assays.

Potential for new GFAP 'context of use' in TBI monitoring

Our sequence-defined GFAP degradome and connected cytological data support possible future clinical applications of GFAP in longitudinal TBI patient monitoring. Three interrelated potential COU areas are considered: *(1) Longitudinal monitoring*; (*2) Astrocyte degeneration and secondary injury; (3) Outcome prognosis*.

(1) Longitudinal GFAP monitoring and influence of age

Tracking GFAP degradation kinetics offers a longitudinal window for TBI patient monitoring during intensive care and for early clinical trial endpoints [2, 11, 38, 56, 74, 96, 134, 169]. GFAP-BDPs dominate in circulation, while CSF carries both, uncleaved GFAP and BDPs [54, 120, 173]. Temporal GFAP profiles with injury day peak (uncleaved and large GFAP-BDPs) are shared with other rapidly degrading TBI biomarkers

including UCH-L1, S100β, brain lipid binding protein, also called FABP7, neuron-specific enolase and SBDPs [54, 158]. These biomarkers have different half-lives, yet share primary injury-related peaks reflecting on the extent of acute mechanoporation, force-triggered filament breakage and calcium-driven initiation proteolysis [54, 85, 90, 119, 126, 137].

Secondary elevation of GFAP-BDPs, particularly of small BDPs involving caspase activation, is seen in a subset of TBI patients. This pattern aligns with previous reports of delayed serum GFAP peaks in a subset of older TBI patients with high CT burden, poor outcome, high mortality and pathophysiological features of more severe TBI [132]. Here CSF measured GFAP-BDP levels are also elevated with age. Age-related increases in baseline GFAP and neurofilament light are linked to reduced clearance or ongoing atrophy [25, 32, 46, 148, 171]. Elderly suffering a TBI clear CSF less efficiently through decreased CSF pulsation, ependymal cilia vulnerability, and disrupted cerebral blood flow affecting biomarker levels [17, 71, 163]. GFAP-BDP monitoring could add informing on secondary TBI pathophysiology.

(2) Detecting astrocyte pathology to inform on secondary injury

Patient-specific secondary GFAP-BDP release during injury progression TBI progresses Neuroimaging reports contusions expanding into peri-lesional tissue attributed to cytotoxic edema already stated above [8, 111, 147, 168]. Cytotoxic edema is characterized by microstructural changes of astrocyte swelling and subsequent integrity loss driven by ion dysregulation and metabolic depletion [21, 151, 153]. These interrelated mechanisms may underlie the variable secondary increases in cell death-associated BDPs observed in a subset of TBI patients. Consistent with this interpretation, progressive astrocyte degeneration is quantified in autopsy brains of TBI patients and shows reduced astrocyte numbers between acute (<6h) and subacute (>6hrs to 3PID) postmortem intervals in cerebral white matter and hippocampus [87]. Thus, GFAP-BDP profiling may indicate secondary adverse postinjury events after TBI.

(3) GFAP-BDP trajectories for TBI outcome prognosis

Elevated GFAP is recognized as prognostic marker after severe TBI [54, 76, 79, 115, 122, 132]. Our findings indicate that timecourse of GFAP degradation -not uncleaved GFAP or large fragments- best distinguish poor versus good 6-months outcome. Being robust to the way the score is dichotomized matters, as defining “good” recovery is inherently personal [159]. The results suggest that ongoing injury-driven GFAP proteolysis offers prognostic insights compared to initial impact-driven uncleaved and end-clipped GFAP levels. This aligns with broader clinical knowledge that early injury progression rather than initial status, shape recovery [15, 165]. Current FDA-approved GFAP testing focuses on a narrow admission window and therefore misses this critical dynamic as longitudinal monitoring is not part of the present FDA approved COU [76, 160]. While GFAP assays may include detecting BDPs, there is no proteoform differentiation.

This study has several limitations

This clinical cohort was relatively small, and some patients had incomplete longitudinal data, due to staffing and logistical constraints during the Covid pandemic. Statistical power was limited but steps to remedy this included truncating at 10PIDs, avoiding imbalanced variance, and use of adequate effect size types. Cohen’s D was used to predict good versus poor outcomes, as AUC modeling was inadequate for simultaneously including elapsed postinjury time. Technical restrictions limited serum MS sequencing. CSF collection in TBI patients undergoing ventriculostomy offers unique biomarker insights yet does carry a small risk of infections [64, 114]. Donated fetal brain specimen limited comparison across donors and conditions. Live-fluorescence reporters limit the use of high-intensity illumination or repeated imaging yet enabled simultaneous monitoring of proteolysis and cell integrity. Despite these challenges, all key measurements were comprehensive across samples using adequate quantification standards and unbiased approaches. Importantly, findings were cross-validated using independent experimental approaches. As this is a discovery-focused study, rigorous orthogonal validation corroborates and supports the reliability of the results. Certainly, larger standardized cohorts and models will be critical for future studies to confirm and extend these findings.

Translational significance and future directions

Collectively, our data position GFAP-BDPs as molecular indicators of disrupted proteostasis and astrocyte pathology. Serial monitoring of these GFAP-BDPs may further individualized patient monitoring with potential relation to physiological parameters in neurocritical care, help detect secondary adverse events, and could improve recovery prognosis in TBI. By linking GFAP fluid profiles to latent proteinopathy, our findings facilitate translational research and support a new framework for TBI phenotyping that may benefit TBI patient care.

FIGURE LEGENDS

Thumbnail: Astrocyte injury states with distinct GFAP proteoforms and fates after TBI

The infographic summarizes four distinct coexisting progressive injury states of human astrocytes after traumatic injury, each defined by unique astrocyte morphologies and GFAP proteoforms and distributions. Key pathways of GFAP post-translational modification, degradation and aggregation are linked to astrocyte dysfunction and underpin fluid biomarker signatures. The illustrated steps provide interpretation linking astrocyte pathology with GFAP biomarker profiles to support Neuro-ICU patient monitoring. ***(1) Uninjured***, healthy astrocyte: Intact plasma membrane and assembled GFAP filaments. ***(2) Mechanoporated***, wounded astrocyte: Mechanical forces cause membrane poration and process beading (clasmatodendrosis), leading to calcium influx and filaments disassembly into monomers (black) and fragments. Proteolytic degradation is initiated by calpains into large fragments (gray), followed by caspases and other proteases into coil1-BDPs that are readily fluid-released (red) and coil2-BDPs that form PTM-decorated aggregates (purple). ***(3) Dystrophic,*** swollen (oncotic) astrocyte shows vacuoles, membrane blebbing and advanced process damage with accumulated PTM-modified GFAP granules marked by citrullination (green) and acetylation (brown) that represent a trauma-related GFAP proteinopathy. ***(4) Necrotic,*** dying astrocyte with integrity loss membrane rupture and lysis, releasing modified coil2-BDPs as markers of irreversible cell loss.

Fig. 1 Variable endings and abundance of small GFAP-BDPs in TBI patients' CSF

A) Sequences of GFAP breakdown products (BDP) with peptide maps and percent coverage of mass spectrometry (MS) of immunoprecipitated GFAP of four cut out gel bandsets from six CSF TBI samples (I.-IV., Supplement Fig.S1). Shown are high confidence peptides (green, FDR$\leq$1%) and repeatedly identified medium confidence peptides (yellow FDR$\leq$5%). ***Bands (I.)*** had 359 amino acids (aa) with calculated molecular weight of 41.7kDa and suggested new N- and C-termini of serine 53 (S53) and lysine 411 (K411). ***Bands (II.)*** spanned 349aa from glycine 56 (G56) to leucine (L404) within which 37/38kDa fragments with variable endings between TBI samples were located (Supplement Figure 1). ***Bands (III.)*** contained two GFAP-BDPs, a 92% covered coil1-containing product of 185aa with calculated molecular weight of 21.8kDa; and a 77% covered coil2-containing product of 151 aa and peptides with estimated molecular weight of 17.5kDa. ***Bands (IV.)*** contained a 96% covered 181 aa coil1 product with size between 21-21.6kDa -±PTMs; and a 77% covered coil2 product of 130aa with estimated molecular weight of 15-15.3kDa. **B)** GFAP immunoblots TBI CSF samples of one and three postinjury days (PIDs) detected by a polyclonal (top) and a monoclonal (clone 3E10, bottom) antibody. The TBI patient was an 84-year-old male sustaining facial fractures, subarachnoid and intraventricular hemorrhage and intraparenchymal hematomas from a fall. Observed GFAP molecular weights were *bands (I.)* 40-42kDa, *(II.)* 36-39kDa, *(III.)* 20.4-23kDa, and bands *(IV.)*, 17-19kDa detected only by the polyclonal antibody. **C)** Predicted endings of small GFAP-BDPs in TBI. ***Coil1 products*** had N-termini serine S53 and alanine A55 and C-termini were arginine R239 and alanine A233. ***Coil2 products*** had consistent N-terminus phenylalanine F261, and ended with either lysine K411 or arginine R390. Different endings were sequenced from different bands of excised gel slices as indicated by the brackets. **D)** Label-free MS quantification documents peptide detection frequency of

coil1 (59± 29%) and coil2 (13±7%) product peptides in eleven MS runs of Bands (III) and (IV.). The difference of peptide detection frequency between the two coils was significant, using mixed model testing ($p<0.0004$; with patient ID as random effect two-tailed T-test with unequal variances, $p=0.00038$).

Fig. 2 Longitudinal tracking of GFAP proteolysis in TBI patients' CSF with shared peaks and individual profiles

A) GFAP immunoblot of serial CSF samples over four postinjury days from a 40-year-old male TBI patients (admission GCS 3, GOSE 8) displays highest GFAP and fragment levels at six hours with additional peaks on PIDs 2-4. **B)** GFAP immunoblot shows serial TBI CSF samples over PIDs 4-10 (a 48-year-old male TBI patient; admission GCS 10, GOSE 6) shows over time declining levels of 37-50kDa and later variably increasing 15-26kDa BDPs. Calibrants: Human recombinant full-length GFAP (50kDa) and his-GFAP-BDP (25kDa). **C-H:** Ten-day profiles of GFAP total **(C),** uncleaved **(D)** and fragment sets **(E-H)** in TBI CSF of 23 TBI patients (102 samples) and resampled mean cubic splines with 95% CI bounds. Graphed are log-transformed calibrated concentrations of subsaturated band densities (calibration curves and scaled exposure densitometry see Supplement Table S4, Fig.S5). Total GFAP, uncleaved, large and small fragments (45-49; 15-19kDa) had significant injury day peaks shown with Cohen's D effect size on injury day versus overall-times adjusted means (linear mixed model, controlled for random donor and age variance, see Supplement Fig. S7, Table S6 for age covariance). Means of 37-39kDa GFAP fragment levels were above mean until day 3, around mean on days 4-5 and below mean thereafter. Small GFAP-BDPs had larger dispersion shown by IQR, kurtosis and variance (σ) due to either high or absent signals yet had mean secondary elevations on later days.

Fig. 3 Correlation between GFAP uncleaved, fragments and coproducts in TBI CSF

A) Pearson's correlation matrix lists coefficients between uncleaved GFAP and all BDP sets measured in 23 TBI patient's 102 CSF samples. **B)** Bivariate plot of full length (50kDa) GFAP substrate and calpain cleavage products (37-39kDa) using orthogonal fit (R^2 with equal error weights) and FDR-corrected Logworth ($\log_{10}$p-value). **C)** Bivariate plot of GFAP-BDP coproducts correlated weaker due to more undetected 15-19kDa versus 20-26kDa bands (circle, 28% 15 more undetected). See Supplement Fig. S8 for all GFAP species bivariate correlations.

Fig. 4 Longitudinal GFAP proteolysis predicts TBI patient outcome, not full-length GFAP

Compared are trajectories of GFAP bandsets over 10 PIDs among TBI patients with good recovery (GOSE 5-8) versus those with poor outcome (GOSE1-4), shown with mean cubic splines and 95% CI bands adjusted for smoothness (21 patients; 95 observations). **A)** Profiles of calpain-derived GFAP fragments (37-39kDa) trajectories differentiated between the two recovery groups by an effect size of 1.1SD ($p=0.02$, Cohen's D adjusted for elapsed time and age effects; subject ID as random effect). **B)** Profiles of small GFAP-BDPs (20-26kDa) showed 0.9SD nonsignificant difference trend between the two groups. **C)** Full-length, 50kDa GFAP profiles overlapped over time between groups lacking prognosis of patient outcome. **D)** Model-adjusted GFAP means with standard errors are shown documenting differences in GFAP fragment levels between TBI patients with good versus poor recovy. See Supplement Table S7 for Cohen's D for effect size of all GFAP species; see Fig. S9 for alternate GOSE partitioning showing similar trends.

Fig. 5 Citrullination and acetylation PTMs are signatures of TBI patients' GFAP fragments

A) MS mapping of posttranslational modifications in GFAP coil1/2-BDPs from six TBI CSF samples. All citrullinations (13, green, including a novel citrullination site at arginine R188), and acetylations (3, brown) were validated by signature ions and mass shifts in MS2 spectra (Supplement Table S8, Fig. S10) with a subset being further confirmed by prior described cell-free peptidylarginine deiminase (PAD) digests, indicated with "*" [65]. Arrows indicate neo-epitopes R270 and R416 for citrullinated-GFAP antibodies [61]. **B)** *Left*: TBI patient-specific citrullinated GFAP-BDP signatures in nine TBI CSF samples show strong BDP signals with rabbit cit-R270-GFAP, and additional larger molecular weight signals using mab CTGF-1221. *Right*:

Unmodified GFAP detected by cloil1 mab3E10 (*top*) or a rabbit polyclonal GFAP (*bottom*) from same samples document proportional differences in unmodified GFAP signals (antibody specifics see Supplement Table S3).

Fig. 6 Novel GFAP cleavage creates coproducts with distinct localization after trauma
Monoclonal antibody mapping confirms MS findings (Fig.1) of GFAP cleavage into two coproduct sets residing in separate compartments after stretch-injury of human cerebral astrocytes [155]: coil1- products were trauma-released whereas coil2-products remained cell-associated. **A)** MS derived coil1/2 sequences for alignment with used antibody epitopes. **B)** Binding regions and defined epitopes of antibody clones within GFAP-BDPs. Mab 3E10 targets coil1B (aa196-217) with stutter motif HEEEVRE (aa204-210) as epitope; 5C10 targets coil 2A (aa240-260) with core epitope (aa257-260) deciphered see Supplement Fig.S10). GA5 binds at the end of coil 2B (aa 374-390) [26]. BD multiclone (4A11, 1B4, 2E1) detects both coils. **C)** Immunoblots of two donor's whole cell lysates (Cells) and concentrated media (Fluid) from control (-) and 2 days post-stretched human astrocyte cultures ("+", 4.8-5.4psi) probed with antibodies from B (color-coded). All clones detected full-length GFAP and large fragments in cells and fluids. Small GFAP-BDPs were in coil-specific different compartments 3E10 detected 20kDa products in fluids but not cells. BD Multiclone detected intracellular 13-28kDa GFAP-BDPs in astrocytes and small bands in extracellular fluids. 5C10 did not detect any small fragments. GA5 detected 17-28kDa GFAP-BDPs in cells, but not in fluids.

Fig. 7 Calpain and caspase activities in compartmental GFAP degradation and astrocyte phenotyping
A) GFAP degradation was analyzed at 48h postinjury across adherend cells, released pool and lifted material with or without calpain and caspase inhibitors. Unstretched and stretch-injured human astrocytes were treated with single or combined inhibitors followed by analysis of lysed adherent cells, concentrated fluids and pelleted lifted material. Calpain-inhibition shows 35-38kDa band reduction in all compartments along with accumulation of uncleaved GFAP in cellular fractions. In contrast, 19-26kDa BDPs were sensitive to both inhibitors across fractions (Quantified in Supplement Fig.S12). **B+C)** Live imaging shows human astrocyte morphotypes and injury stages defined by membrane permeability with calpain and caspase activity during 5-6 hours postinjury. Elongated (*Top*) and bushy (*bottom*) morphotypes had distinct morphologies. Control astrocytes had intact processes with calpain activity (converted substrate CMAC-tBOC-leucyl-methionine, blue). Stretched cultures were mixted population of cells with intact membranes [PI-] or with leaky membranes [PI+] that included dystrophic astrocytes bearing no, thin or beaded clasmatodendrotic processes. Fibrous dystrophic astrocytes were calpain-inactive and caspase-active even when pyknotic (green/yellow). Bushy dystrophic astrocytes displayed calpain and caspase activity (tiel) with a subgroup being membrane permeable, while other integrity compromised bushy cells were devoid of these protease activities that included necrotic cells (red only). Phase-dense vacuoles were unstained (Supplement Fig. S13). Scale bars: 100 µm.

Fig. 8 Trauma induced citrullinated GFAP aggregates in pathological human astrocytes
A) Immunofluorescence of coil2 GFAP (GA5, red) and citrullinated GFAP (cit270-GFAP, green) shows abundant accumulation of non-filamentous citrullinated GFAP clusters at 5 and 24h post-stretching (*right*) compared to hardly any cit-GFAP in controls (*left*). **B)** Unstretched astrocytes (*left*) and three pathological astrocyte morphotypes (right) after stretch-injury: reactive astrocyte with thick, hypertrophied processes, bright cytoskeletal GFAP and fine-grained cytosolic cit-GFAP (yellow); astrocytes with fanning-out processes surrounded by cit-GFAP sprinkles (arrows); dystrophic astrocytes with swollen somata, malformed, cryptic or missing processes bearing various sized cit-GFAP aggregates in absence or presence of non-filamentous or wavy GFAP (arrowheads; see Supplement Figure S14 for individual channels and phase images). Scale bars: 50 µm.

ABBREVIATIONS

Traumatic brain injury (TBI), glial fibrillary acidic protein (GFAP), mass spectrometry (MS), breakdown products (BDPs), cerebrospinal fluid (CSF), Extended Glasgow Outcome Scale (GOSE), posttranslational modifications (PTMs), αII-spectrin breakdown products (SBDPs), context of use (COU), National Institute of Neurological Disorders and Stroke (NINDS), Glasgow Coma Scale (GCS), Institutional Review Board (IRB), Glasgow Outcome Scale (GOS), SDS polyacrylamide gel electrophoresis (SDS-PAGE), mouse monoclonal antibodies (mabs), acetonitrile (ACN), liquid chromatography-tandem MS (LC-MS/MS), full spectra (MS1), higher-energy collisional dissociation (HCD; MS2), Proteome Discoverer (PD), false discovery rate (FDR), peptidylarginine deiminase (PAD), amino acids (aa), Tris-buffered saline with Tween (TBST), room temperature (RT), Enhanced Chemiluminescence (ECL), propidium iodide (PI), Whole cell lysate (WCL, "cells"), Conditioned medium (CM, "fluid"), Research Resource Identifier (RRID), restricted maximum likelihood (REML), linear mixed model (LMM), patient identifier (ID), partial omega squared (ω_p^2), coefficients of variation (CV), fixed effect statistic (F-statistic), degrees of freedom (df), denominator term (DFDen), confidence intervals (CI), postinjury day (PID), adjusted means (Adj.Means), Alzheimer's disease (AD), CMAC-tBOC-leucyl-methionine (CMAC-tBLM), interquartile range (IQR).

ACKNOWLEDGEMENT & FUNDING

FUNDING

Dana Foundation: Clinical Neuroscience "First in man" award # 20182601: "Clinical study and trauma culture model experiments"
Brain Injury Research Center (BIRC), State of California: "Clinical study and trauma culture model experiments"
National Institute of Health, Institute of Neuronal Disorders and Stroke,
NIH/NINDS, R01 NS052831 "Biochemical markers of severe traumatic brain injury"
NIH/NINDS Small Business Innovation Research, SBIR grant # 1R43NS106972-01
"Validation and GFAP proteoform characterization for assay use"
Sponsored Research Agreement, Abbott Diagnostics: "GFAP fragment analyses"
Sponsored Research Agreement, BRAINBox Solutions Inc., Richmond VA, USA: "Validation studies and patent licensing"
Semel Institute IDDRC and Brain Injury Research Center, BIRC, UCLA, Los Angeles, CA, USA. Facilities supplies for cell culture and microscopy work.

ACKNOWLEDGEMENT

The authors acknowledge with appreciation the receipt of mouse antibody CTGF-1221 to citrullinated GFAP (RRID: AB_3678889) that was kindly provided by Dr. Akihito Ishigami, Tokyo Metropolitan Institute of Gerontology, Tokyo, Japan. Special thanks goes to Dr. Sarah Dry and Ko Kiehle Translational Pathology Core lab, Ronald Reagan UCLA Medical Center, and Dr. Angela Chen, Family Planning & UCLA OBGYN Ronald Reagan Medical Center, for consenting and procuring voluntary donated fetal remains as pre-shelved specimen for cerebral tissues. Greatly appreciates for their grateful for input from are Laboratory assistant Kiohei Itamura, and UCLA Honors students Michelle Gong, Raghu Padmanabhuni, Aryana Sargsyan, Ana Karimi Bidhendi, Emerald Wong, Mhina Cham, Aryana Sargsyan, Kunal Ranat; David Sanville, and for the

valuable critical care management assistance provided by Courtney Real and Jesus Ruiz-Tejada and the help from clinical fellow Azim Laiwalla.

REFERENCES

1 Acarin L, Villapol S, Faiz M, Rohn TT, Castellano B, Gonzalez B (2007) Caspase-3 activation in astrocytes following postnatal excitotoxic damage correlates with cytoskeletal remodeling but not with cell death or proliferation. Glia 55: 954-965

2 Adamczak SE, de Rivero Vaccari JP, Dale G, Brand FJ, 3rd, Nonner D, Bullock MR, Dahl GP, Dietrich WD, Keane RW (2014) Pyroptotic neuronal cell death mediated by the AIM2 inflammasome. Journal of cerebral blood flow and metabolism : official journal of the International Society of Cerebral Blood Flow and Metabolism 34: 621-629 Doi 10.1038/jcbfm.2013.236

3 Aleksandrova MA, Sukhinich KK (2022) Astrocytes of the Brain: Retinue Plays the King. Russ J Dev Biol+ 53: 252-271 Doi 10.1134/S1062360422040026

4 Algeciras ME, Takahara H, Bhattacharya SK (2008) Mechanical stretching elevates peptidyl arginine deiminase 2 expression in astrocytes. Curr Eye Res 33: 994-1001 Doi 10.1080/02713680802447113

5 Ammendolia DA, Bement WM, Brumell JH (2021) Plasma membrane integrity: implications for health and disease. BMC Biol 19: 71 Doi 10.1186/s12915-021-00972-y

6 Ashton NJ, Di Molfetta G, Tan K, Blennow K, Zetterberg H, Messing A (2024) Plasma concentrations of glial fibrillary acidic protein, neurofilament light, and tau in Alexander disease. Neurol Sci 45: 4513-4518 Doi 10.1007/s10072-024-07495-8

7 Barbee KA (2005) Mechanical cell injury. Ann N Y Acad Sci 1066: 67-84 Doi 10.1196/annals.1363.006

8 Batista L, Stence NV, Mirsky DM, Lewis T, Graber S, Ghebrechristos HE, Alaghband G, Connery AK, O'Neill BR, Lindberg DM (2025) Cytotoxic edema is associated with injury severity but not abusive mechanism in young children with traumatic brain injury. Child Abuse & Neglect 161: 107312 Doi https://doi.org/10.1016/j.chiabu.2025.107312

9 Battaglia RA, Beltran AS, Delic S, Dumitru R, Robinson JA, Kabiraj P, Herring LE, Madden VJ, Ravinder N, Willems Eet al (2019) Site-specific phosphorylation and caspase cleavage of GFAP are new markers of Alexander disease severity. Elife 8: Doi 10.7554/eLife.47789

10 Baudry M, Bi X (2016) Calpain-1 and Calpain-2: The Yin and Yang of Synaptic Plasticity and Neurodegeneration. Trends Neurosci 39: 235

11 Baudry M, Luo YL, Bi X (2023) Calpain-2 Inhibitors as Therapy for Traumatic Brain Injury. Neurotherapeutics : the journal of the American Society for Experimental NeuroTherapeutics 20: 1592-1602 Doi 10.1007/s13311-023-01407-y

12 Bazarian JJ, Biberthaler P, Welch RD, Lewis LM, Barzo P, Bogner-Flatz V, Gunnar Brolinson P, Buki A, Chen JY, Christenson RHet al (2018) Serum GFAP and UCH-L1 for prediction of absence of intracranial injuries on head CT (ALERT-TBI): a multicentre observational study. The Lancet Neurology 17: 782-789 Doi 10.1016/S1474-4422(18)30231-X

13 Bazarian JJ, Zetterberg H, Buki A, Dengler BA, Diaz-Arrastia R, Korley FK, Lazarus R, Meier TB, Mondello S, Moritz Ket al (2025) Blood-Based Biomarkers for Improved Characterization of Traumatic Brain Injury: Recommendations from the 2024 National Institute for Neurological Disorders and Stroke Traumatic Brain Injury Classification and Nomenclature Initiative Blood-Based Biomarkers Working Group. Journal of neurotrauma: Doi 10.1089/neu.2024.0581

14 Beer R, Franz G, Srinivasan A, Hayes RL, Pike BR, Newcomb JK, Zhao X, Schmutzhard E, Poewe W, Kampfl A (2000) Temporal profile and cell subtype distribution of activated caspase-3 following experimental traumatic brain injury. Journal of neurochemistry 75: 1264-1273

15 Bhattacharyay S, Caruso PF, Åkerlund C, Wilson L, Stevens RD, Menon DK, Steyerberg EW, Nelson DW, Ercole A, the C-TBIiet al (2023) Mining the contribution of intensive care clinical course to outcome after traumatic brain injury. npj Digital Medicine 6: 154 Doi 10.1038/s41746-023-00895-8

16 Block J, Witt H, Candelli A, Peterman EJ, Wuite GJ, Janshoff A, Koster S (2017) Nonlinear Loading-Rate-Dependent Force Response of Individual Vimentin Intermediate Filaments to Applied Strain. Phys Rev Lett 118: 048101 Doi 10.1103/PhysRevLett.118.048101

17 Bolte AC, Dutta AB, Hurt ME, Smirnov I, Kovacs MA, McKee CA, Ennerfelt HE, Shapiro D, Nguyen BH, Frost ELet al (2020) Meningeal lymphatic dysfunction exacerbates traumatic brain injury pathogenesis. Nature Communications 11: 4524 Doi 10.1038/s41467-020-18113-4

18 Bondarenko A, Chesler M (2001) Calcium dependence of rapid astrocyte death induced by transient hypoxia, acidosis, and extracellular ion shifts. Glia 34: 143-149

19 Bons JA, Michielsen EC, de Boer D, Bouwman FG, Jaeken J, van Dieijen-Visser MP, Rubio-Gozalbo ME, Wodzig WK (2008) A specific immunoprecipitation method for isolating isoforms of insulin-like growth factor binding protein-3 from serum. Clin Chim Acta 387: 59-65 Doi 10.1016/j.cca.2007.09.002

20 Brett BL, Gardner RC, Godbout J, Dams-O'Connor K, Keene CD (2022) Traumatic Brain Injury and Risk of Neurodegenerative Disorder. Biological psychiatry 91: 498-507 Doi 10.1016/j.biopsych.2021.05.025

21 Bullock R, Maxwell WL, Graham DI, Teasdale GM, Adams JH (1991) Glial swelling following human cerebral contusion: an ultrastructural study. Journal of neurology, neurosurgery, and psychiatry 54: 427-434

22 Byun Y, Chen F, Chang R, Trivedi M, Green KJ, Cryns VL (2001) Caspase cleavage of vimentin disrupts intermediate filaments and promotes apoptosis. Cell death and differentiation 8: 443-450 Doi 10.1038/sj.cdd.4400840

23 Caballero B, Bourdenx M, Luengo E, Diaz A, Sohn PD, Chen X, Wang C, Juste YR, Wegmann S, Patel Bet al (2021) Acetylated tau inhibits chaperone-mediated autophagy and promotes tau pathology propagation in mice. Nature Communications 12: 2238 Doi 10.1038/s41467-021-22501-9

24 Cao X, Zhang Y, Zou L, Xiao H, Chu Y, Chu X (2010) Persistent oxygen-glucose deprivation induces astrocytic death through two different pathways and calpain-mediated proteolysis of cytoskeletal proteins during astrocytic oncosis. Neuroscience letters 479: 118-122 Doi 10.1016/j.neulet.2010.05.040

25 Chen CP, Chen RL, Preston JE (2010) The influence of cerebrospinal fluid turnover on age-related changes in cerebrospinal fluid protein concentrations. Neuroscience letters 476: 138-141 Doi 10.1016/j.neulet.2010.04.015

26 Chen MH, Hagemann TL, Quinlan RA, Messing A, Perng MD (2013) Caspase cleavage of GFAP produces an assembly-compromised proteolytic fragment that promotes filament aggregation. ASN neuro 5: e00125 Doi 10.1042/AN20130032

27 Chen W, Nishikimi A, Kamata T, Adachi Y (2006) A reducing and denaturing step maximizes the immunoprecipitations of m-calpain and I-2(PP2A)/SET: an approach toward antibodies that do not work well in immunoprecipitation. J Biochem Biophys Methods 68: 65-68 Doi 10.1016/j.jbbm.2006.02.012

28 Chen YS, Lim SC, Chen MH, Quinlan RA, Perng MD (2011) Alexander disease causing mutations in the C-terminal domain of GFAP are deleterious both to assembly and network formation with the potential to both activate caspase 3 and decrease cell viability. Exp Cell Res 317: 2252-2266 Doi 10.1016/j.yexcr.2011.06.017

29 Chu X, Fu X, Zou L, Qi C, Li Z, Rao Y, Ma K (2007) Oncosis, the possible cell death pathway in astrocytes after focal cerebral ischemia. Brain research 1149: 157-164 Doi 10.1016/j.brainres.2007.02.061

30 Ciesielski-Treska J, Goetschy JF, Aunis D (1984) Proteolytic degradation of vimentin and glial fibrillary acidic protein in rat astrocytes in primary culture. European journal of biochemistry / FEBS 138: 465-471

31 Colombo JA, Yanez A, Lipina SJ (1997) Interlaminar astroglial processes in the cerebral cortex of non human primates: response to injury. J Hirnforsch 38: 503-512

32 Cooper JG, Stukas S, Ghodsi M, Ahmed N, Diaz-Arrastia R, Holmes DT, Wellington CL (2023) Age specific reference intervals for plasma biomarkers of neurodegeneration and neurotrauma in a Canadian population. Clinical biochemistry 121-122: 110680 Doi 10.1016/j.clinbiochem.2023.110680

33 DeArmond SJ, Fajardo M, Naughton SA, Eng LF (1983) Degradation of glial fibrillary acidic protein by a calcium dependent proteinase: an electroblot study. Brain research 262: 275-282

34 Deng Y, Thompson BM, Gao X, Hall ED (2007) Temporal relationship of peroxynitrite-induced oxidative damage, calpain-mediated cytoskeletal degradation and neurodegeneration after traumatic brain injury. Experimental neurology 205: 154-165 Doi 10.1016/j.expneurol.2007.01.023

35 Der Perng M, Su M, Wen SF, Li R, Gibbon T, Prescott AR, Brenner M, Quinlan RA (2006) The Alexander disease-causing glial fibrillary acidic protein mutant, R416W, accumulates into Rosenthal fibers by a pathway that involves filament aggregation and the association of alpha B-crystallin and HSP27. Am J Hum Genet 79: 197-213 Doi 10.1086/504411

36 Dias C, Nylandsted J (2021) Plasma membrane integrity in health and disease: significance and therapeutic potential. Cell Discovery 7: 4 Doi 10.1038/s41421-020-00233-2

37 Diaz-Arrastia R (2024) Performance of Diagnostic Biomarkers for Traumatic Brain Injury Within the First Hour-Expanding Their Clinical Utility. JAMA Netw Open 7: e2431102 Doi 10.1001/jamanetworkopen.2024.31102

38 Diaz-Arrastia R, Kochanek PM, Bergold P, Kenney K, Marx CE, Grimes CJ, Loh LT, Adam LT, Oskvig D, Curley KCet al (2014) Pharmacotherapy of traumatic brain injury: state of the science and the road forward: report of the Department of Defense Neurotrauma Pharmacology Workgroup. Journal of neurotrauma 31: 135-158 Doi 10.1089/neu.2013.3019

39 Dobson J, Kumar A, Willis LF, Tuma R, Higazi DR, Turner R, Lowe DC, Ashcroft AE, Radford SE, Kapur Net al (2017) Inducing protein aggregation by extensional flow. Proceedings of the National Academy of Sciences 114: 4673-4678 Doi doi:10.1073/pnas.1702724114
40 Ekert PG, Silke J, Vaux DL (1999) Caspase inhibitors. Cell death and differentiation 6: 1081-1086 Doi 10.1038/sj.cdd.4400594
41 Escartin C, Galea E, Lakatos A, O'Callaghan JP, Petzold GC, Serrano-Pozo A, Steinhauser C, Volterra A, Carmignoto G, Agarwal Aet al (2021) Reactive astrocyte nomenclature, definitions, and future directions. Nat Neurosci 24: 312-325 Doi 10.1038/s41593-020-00783-4
42 Farkas O, Lifshitz J, Povlishock JT (2006) Mechanoporation induced by diffuse traumatic brain injury: an irreversible or reversible response to injury? The Journal of neuroscience : the official journal of the Society for Neuroscience 26: 3130-3140
43 Fereidoni M, Sabouni F, Moghimi A, Hosseini S (2013) The effects of trypsin on rat brain astrocyte activation. Iran J Neurol 12: 129-135
44 Gae DD, Budamagunta MS, Hess JF, McCarrick RM, Lorigan GA, FitzGerald PG, Voss JC (2019) Completion of the Vimentin Rod Domain Structure Using Experimental Restraints: A New Tool for Exploring Intermediate Filament Assembly and Mutations. Structure 27: 1547-1560.e1544 Doi 10.1016/j.str.2019.07.011
45 Gafni J, Cong X, Chen SF, Gibson BW, Ellerby LM (2009) Calpain-1 cleaves and activates caspase-7. The Journal of biological chemistry 284: 25441-25449 Doi 10.1074/jbc.M109.038174
46 Gardner RC, Dams-O'Connor K, Morrissey MR, Manley GT (2017) Geriatric Traumatic Brain Injury: Epidemiology, Outcomes, Knowledge Gaps, and Future Directions. Journal of neurotrauma 35: 889-906 Doi 10.1089/neu.2017.5371
47 Giza CC, Hovda DA (2014) The new neurometabolic cascade of concussion. Neurosurgery 75 Suppl 4: S24-33 Doi 10.1227/NEU.0000000000000505
48 GOLL DE, THOMPSON VF, LI H, WEI W, CONG J (2003) The Calpain System. Physiological Reviews 83: 731-801 Doi 10.1152/physrev.00029.2002
49 Guan Y, Zhu Q, Huang D, Zhao S, Jan Lo L, Peng J (2015) An equation to estimate the difference between theoretically predicted and SDS PAGE-displayed molecular weights for an acidic peptide. Scientific reports 5: 13370 Doi 10.1038/srep13370
50 Guo J, Yang WT, Mai FY, Liang JR, Luo J, Zhou MC, Yu DD, Wang YL, Li CG (2024) Unravelling oncosis: morphological and molecular insights into a unique cell death pathway. Front Immunol 15: 1450998 Doi 10.3389/fimmu.2024.1450998
51 Gupta R, Sahu M, Srivastava D, Tiwari S, Ambasta RK, Kumar P (2021) Post-translational modifications: Regulators of neurodegenerative proteinopathies. Ageing Res Rev 68: 101336 Doi 10.1016/j.arr.2021.101336
52 Habshah M, Sani M, Arasan J (2018) Robust Heteroscedasticity Consistent Covariance Matrix Estimator based on Robust Mahalanobis Distance and Diagnostic Robust Generalized Potential Weighting Methods in Linear Regression. J Mod Appl Stat Meth 17: Doi ARTN 1710.22237/jmasm/1530279855
53 Hagemann TL, Boelens WC, Wawrousek EF, Messing A (2009) Suppression of GFAP toxicity by alphaB-crystallin in mouse models of Alexander disease. Human molecular genetics 18: 1190-1199 Doi 10.1093/hmg/ddp013
54 Halford J, Shen S, Itamura K, Levine J, Chong AC, Czerwieniec G, Glenn TC, Hovda DA, Vespa P, Bullock Ret al (2017) New astroglial injury-defined biomarkers for neurotrauma assessment. Journal of cerebral blood flow and metabolism : official journal of the International Society of Cerebral Blood Flow and Metabolism 37: 3278-3299 Doi 10.1177/0271678X17724681
55 Han K-K, Richard C, Biserte G (1983) Current developments in chemical cleavage of proteins. International Journal of Biochemistry 15: 875-884 Doi https://doi.org/10.1016/0020-711X(83)90162-3
56 Harter L, Keel M, Hentze H, Leist M, Ertel W (2001) Caspase-3 activity is present in cerebrospinal fluid from patients with traumatic brain injury. Journal of neuroimmunology 121: 76-78
57 Heaven MR, Flint D, Randall SM, Sosunov AA, Wilson L, Barnes S, Goldman JE, Muddiman DC, Brenner M (2016) Composition of Rosenthal Fibers, the Protein Aggregate Hallmark of Alexander Disease. Journal of proteome research 15: 2265-2282 Doi 10.1021/acs.jproteome.6b00316
58 Hinkle DA, Baldwin SA, Scheff SW, Wise PM (1997) GFAP and S100beta expression in the cortex and hippocampus in response to mild cortical contusion. Journal of neurotrauma 14: 729-738
59 Hsu JC, Nelson B (1998) Multiple comparisons in the general linear model. J Comput Graph Stat 7: 23-41 Doi Doi 10.2307/1390767
60 Inekci D, Jonesco DS, Kennard S, Karsdal MA, Henriksen K (2015) The potential of pathological protein fragmentation in blood-based biomarker development for dementia - with emphasis on Alzheimer's disease. Frontiers in neurology 6: 90 Doi 10.3389/fneur.2015.00090
61 Ishigami A, Masutomi H, Handa S, Nakamura M, Nakaya S, Uchida Y, Saito Y, Murayama S, Jang B, Jeon YCet al (2015) Mass spectrometric identification of citrullination sites and immunohistochemical detection of citrullinated glial fibrillary acidic protein in Alzheimer's disease brains. Journal of neuroscience research 93: 1664-1674 Doi 10.1002/jnr.23620

62 Ishigami A, Ohsawa T, Hiratsuka M, Taguchi H, Kobayashi S, Saito Y, Murayama S, Asaga H, Toda T, Kimura Net al (2005) Abnormal accumulation of citrullinated proteins catalyzed by peptidylarginine deiminase in hippocampal extracts from patients with Alzheimer's disease. Journal of neuroscience research 80: 120-128 Doi 10.1002/jnr.20431
63 Jany PL, Agosta GE, Benko WS, Eickhoff JC, Keller SR, Köehler W, Koeller D, Mar S, Naidu S, Marie Ness Jet al (2015) CSF and Blood Levels of GFAP in Alexander Disease. eneuro 2: ENEURO.0080-0015.2015 Doi 10.1523/eneuro.0080-15.2015
64 Jha RM, Kochanek PM, Simard JM (2019) Pathophysiology and treatment of cerebral edema in traumatic brain injury. Neuropharmacology 145: 230-246 Doi 10.1016/j.neuropharm.2018.08.004
65 Jin Z, Fu Z, Yang J, Troncosco J, Everett AD, Van Eyk JE (2013) Identification and characterization of citrulline-modified brain proteins by combining HCD and CID fragmentation. Proteomics 13: 2682-2691 Doi 10.1002/pmic.201300064
66 Jones JR, Kong L, Hanna MGt, Hoffman B, Krencik R, Bradley R, Hagemann T, Choi J, Doers M, Dubovis Met al (2018) Mutations in GFAP Disrupt the Distribution and Function of Organelles in Human Astrocytes. Cell Rep 25: 947-958.e944 Doi 10.1016/j.celrep.2018.09.083
67 Kabir F, Atkinson R, Cook AL, Phipps AJ, King AE (2023) The role of altered protein acetylation in neurodegenerative disease. Frontiers in Aging Neuroscience 14: Doi 10.3389/fnagi.2022.1025473
68 Karamian A, Lucke-Wold B, Seifi A (2024) Prevalence of Traumatic Brain Injury in the General Adult Population of the USA: A Meta-Analysis. Neuroepidemiology: 1-10 Doi 10.1159/000540676
69 Kilinc D, Gallo G, Barbee KA (2009) Mechanical membrane injury induces axonal beading through localized activation of calpain. Experimental neurology 219: 553-561 Doi 10.1016/j.expneurol.2009.07.014
70 Kim B, Kim S, Jin MS (2018) Crystal structure of the human glial fibrillary acidic protein 1B domain. Biochemical and biophysical research communications 503: 2899-2905 Doi 10.1016/j.bbrc.2018.08.066
71 Kim JH, Im JG, Park SH (2024) Measurement of changes in cerebrospinal fluid pulsation after traumatic brain injury using echo-planar imaging-based functional MRI. NMR in biomedicine 37: e5061 Doi 10.1002/nbm.5061
72 Kim JH, Kwon SJ, Stankewich MC, Huh GY, Glantz SB, Morrow JS (2016) Reactive protoplasmic and fibrous astrocytes contain high levels of calpain-cleaved alpha 2 spectrin. Exp Mol Pathol 100: 1-7 Doi 10.1016/j.yexmp.2015.11.005
73 Knoblach SM, Alroy DA, Nikolaeva M, Cernak I, Stoica BA, Faden AI (2004) Caspase inhibitor z-DEVD-fmk attenuates calpain and necrotic cell death in vitro and after traumatic brain injury. Journal of cerebral blood flow and metabolism : official journal of the International Society of Cerebral Blood Flow and Metabolism 24: 1119-1132 Doi 10.1097/01.WCB.0000138664.17682.32
74 Knoblach SM, Nikolaeva M, Huang X, Fan L, Krajewski S, Reed JC, Faden AI (2002) Multiple caspases are activated after traumatic brain injury: evidence for involvement in functional outcome. Journal of neurotrauma 19: 1155-1170 Doi 10.1089/08977150260337967
75 Korley F, Pauls Q, Yeatts SD, Jones CMC, Corbett-Valade E, Silbergleit R, Frankel M, Barsan W, Cahill ND, Bazarian JJet al (2021) Progesterone Treatment Does Not Decrease Serum Levels of Biomarkers of Glial and Neuronal Cell Injury in Moderate and Severe Traumatic Brain Injury Subjects: A Secondary Analysis of the Progesterone for Traumatic Brain Injury, Experimental Clinical Treatment (ProTECT) III Trial. J Neurotrauma 38: 1953
76 Korley FK, Jain S, Sun X, Puccio AM, Yue JK, Gardner RC, Wang KKW, Okonkwo DO, Yuh EL, Mukherjee Pet al (2022) Prognostic value of day-of-injury plasma GFAP and UCH-L1 concentrations for predicting functional recovery after traumatic brain injury in patients from the US TRACK-TBI cohort: an observational cohort study. The Lancet Neurology 21: 803-813 Doi 10.1016/S1474-4422(22)00256-3
77 Kouklis PD, Traub P, Georgatos SD (1992) Involvement of the consensus sequence motif at coil 2b in the assembly and stability of vimentin filaments. Journal of cell science 102 (Pt 1): 31-41 Doi 10.1242/jcs.102.1.31
78 Kroes ADA, Finley JR (2023) Demystifying omega squared: Practical guidance for effect size in common analysis of variance designs. Psychol Methods: Doi 10.1037/met0000581
79 Kulbe JR, Jain S, Nelson LD, Korley FK, Mukherjee P, Sun X, Okonkwo DO, Giacino JT, Vassar MJ, Robertson CSet al (2022) Association of day-of-injury plasma glial fibrillary acidic protein concentration and six-month posttraumatic stress disorder in patients with mild traumatic brain injury. Neuropsychopharmacology 47: 2300-2308 Doi 10.1038/s41386-022-01359-5
80 Lakens D (2013) Calculating and reporting effect sizes to facilitate cumulative science: a practical primer for t-tests and ANOVAs. Frontiers in Psychology 4: Doi 10.3389/fpsyg.2013.00863
81 Lakshmi R, Sajesh TA (2025) A robust distance-based approach for detecting multidimensional outliers. J Appl Stat 52: 1278-1298 Doi 10.1080/02664763.2024.2422403
82 Lazarus RC, Buonora JE, Flora MN, Freedy JG, Holstein GR, Martinelli GP, Jacobowitz DM, Mueller GP (2015) Protein Citrullination: A Proposed Mechanism for Pathology in Traumatic Brain Injury. Frontiers in neurology 6: Doi 10.3389/fneur.2015.00204
83 Lee MS, Kwon YT, Li M, Peng J, Friedlander RM, Tsai LH (2000) Neurotoxicity induces cleavage of p35 to p25 by calpain. Nature 405: 360-364 Doi 10.1038/35012636
84 Lee YB, Du S, Rhim H, Lee EB, Markelonis GJ, Oh TH (2000) Rapid increase in immunoreactivity to GFAP in astrocytes in vitro induced by acidic pH is mediated by calcium influx and calpain I. Brain research 864: 220-229

85 Levine J, Kwon E, Paez P, Yan W, Czerwieniec G, Loo JA, Sofroniew MV, Wanner IB (2015) Traumatically injured astrocytes release a proteomic signature modulated by STAT3-dependent cell survival. Glia: Doi 10.1002/glia.22953
86 Levine J, Kwon E, Sondej M, Paez P, Czerwieniec G, Ao Y, Sofroniew MV, Loo JA, Wanner IB (2016) Traumatically injured astrocytes release a proteomic signature modulated by STAT3 dependent cell survival. Glia 64: 668-694 Doi 10.1002/glia.22953
87 Li DR, Zhang F, Wang Y, Tan XH, Qiao DF, Wang HJ, Michiue T, Maeda H (2012) Quantitative analysis of GFAP- and S100 protein-immunopositive astrocytes to investigate the severity of traumatic brain injury. Leg Med (Tokyo) 14: 84-92 Doi 10.1016/j.legalmed.2011.12.007
88 Lin NH, Jian WS, Snider N, Perng MD (2024) Glial fibrillary acidic protein is pathologically modified in Alexander disease. The Journal of biological chemistry 300: 107402 Doi 10.1016/j.jbc.2024.107402
89 Lin NH, Yang AW, Chang CH, Perng MD (2021) Elevated GFAP isoform expression promotes protein aggregation and compromises astrocyte function. FASEB journal : official publication of the Federation of American Societies for Experimental Biology 35: e21614 Doi 10.1096/fj.202100087R
90 Lisi I, Moro F, Mazzone E, Marklund N, Pischiutta F, Kobeissy F, Mao X, Corrigan F, Helmy A, Nasrallah Fet al (2024) Exploiting blood-based biomarkers to align preclinical models with human traumatic brain injury. Brain : a journal of neurology: Doi 10.1093/brain/awae350
91 Liu G-Y, Xie W-L, Wang Y-T, Chen L, Xu Z-Z, Lv Y, Wu Q-P (2023) Calpain: the regulatory point of myocardial ischemia-reperfusion injury. Frontiers in Cardiovascular Medicine Volume 10 - 2023: Doi 10.3389/fcvm.2023.1194402
92 Loh KY, Wang Z, Liao P (2019) Oncotic Cell Death in Stroke. Rev Physiol Biochem Pharmacol 176: 37-64 Doi 10.1007/112_2018_13
93 Lumpkins KM, Bochicchio GV, Keledjian K, Simard JM, McCunn M, Scalea T (2008) Glial fibrillary acidic protein is highly correlated with brain injury. The Journal of trauma 65: 778-782; discussion 782-774
94 Maas AIR, Menon DK, Manley GT, Abrams M, Åkerlund C, Andelic N, Aries M, Bashford T, Bell MJ, Bodien YGet al (2022) Traumatic brain injury: progress and challenges in prevention, clinical care, and research. The Lancet Neurology 21: 1004-1060 Doi https://doi.org/10.1016/S1474-4422(22)00309-X
95 Machnicka B, Ponceau A, Picot J, Colin Y, Lecomte MC (2020) Deficiency of αII-spectrin affects endothelial cell-matrix contact and migration leading to impairment of angiogenesis in vitro. Cell Mol Biol Lett 25: 3 Doi 10.1186/s11658-020-0200-y
96 Madias MI, Stessman LN, Warlof SJ, Kudryashev JA, Kwon EJ (2024) Spatial Measurement and Inhibition of Calpain Activity in Traumatic Brain Injury with an Activity-Based Nanotheranostic Platform. ACS Nano 18: 25565-25576 Doi 10.1021/acsnano.4c06052
97 Majno G, Joris I (1995) Apoptosis, oncosis, and necrosis. An overview of cell death. The American journal of pathology 146: 3-15
98 Manley GT, Dams-O'Connor K, Alosco ML, Awwad HO, Bazarian JJ, Bragge P, Corrigan JD, Doperalski A, Ferguson AR, Mac Donald CLet al (2025) A new characterisation of acute traumatic brain injury: the NIH-NINDS TBI Classification and Nomenclature Initiative. The Lancet Neurology 24: 512-523 Doi 10.1016/S1474-4422(25)00154-1
99 Mavroudis I, Kazis D, Petridis FE, Balmus IM, Papaliagkas V, Ciobica A (2024) The Association Between Traumatic Brain Injury and the Risk of Cognitive Decline: An Umbrella Systematic Review and Meta-Analysis. Brain Sci 14: Doi 10.3390/brainsci14121188
100 McMahon PJ, Panczykowski DM, Yue JK, Puccio AM, Inoue T, Sorani MD, Lingsma HF, Maas AI, Valadka AB, Yuh ELet al (2015) Measurement of the glial fibrillary acidic protein and its breakdown products GFAP-BDP biomarker for the detection of traumatic brain injury compared to computed tomography and magnetic resonance imaging. Journal of neurotrauma 32: 527-533 Doi 10.1089/neu.2014.3635
101 Messing A, Brenner M (2020) GFAP at 50. ASN neuro 12: 1759091420949680 Doi 10.1177/1759091420949680
102 Messing A, Goldman JE, Johnson AB, Brenner M (2001) Alexander Disease: New Insights From Genetics. Journal of Neuropathology & Experimental Neurology 60: 563-573 Doi 10.1093/jnen/60.6.563
103 Metting Z, Wilczak N, Rodiger LA, Schaaf JM, van der Naalt J (2012) GFAP and S100B in the acute phase of mild traumatic brain injury. Neurology 78: 1428-1433 Doi 10.1212/WNL.0b013e318253d5c7
104 Metwally E, Al-Abbadi HA, Hussain T, Murtaza G, Abdellatif AM, Ahmed MF (2023) Calpain signaling: from biology to therapeutic opportunities in neurodegenerative disorders. Front Vet Sci 10: 1235163 Doi 10.3389/fvets.2023.1235163
105 Michielsen EC, Diris JH, Hackeng CM, Wodzig WK, Van Dieijen-Visser MP (2005) Highly sensitive immunoprecipitation method for extracting and concentrating low-abundance proteins from human serum. Clinical chemistry 51: 222-224 Doi 10.1373/clinchem.2004.036251
106 Mouser PE, Head E, Ha KH, Rohn TT (2006) Caspase-mediated cleavage of glial fibrillary acidic protein within degenerating astrocytes of the Alzheimer's disease brain. The American journal of pathology 168: 936-946 Doi 10.2353/ajpath.2006.050798
107 Muñoz-Ballester C, Robel S (2023) Astrocyte-mediated mechanisms contribute to traumatic brain injury pathology. WIREs Mech Dis 15: e1622 Doi 10.1002/wsbm.1622

108 Nelson LD, Temkin NR, Barber J, Brett BL, Okonkwo DO, McCrea MA, Giacino JT, Bodien YG, Robertson C, Corrigan JDet al (2023) Functional Recovery, Symptoms, and Quality of Life 1 to 5 Years After Traumatic Brain Injury: Findings From the TRACK-TBI Study. JAMA Network Open 6: e233660-e233660 Doi 10.1001/jamanetworkopen.2023.3660
109 Nelson LD, Temkin NR, Dikmen S, Barber J, Giacino JT, Yuh E, Levin HS, McCrea MA, Stein MB, Mukherjee Pet al (2019) Recovery After Mild Traumatic Brain Injury in Patients Presenting to US Level I Trauma Centers: A Transforming Research and Clinical Knowledge in Traumatic Brain Injury (TRACK-TBI) Study. JAMA neurology: Doi 10.1001/jamaneurol.2019.1313
110 Nelson PR, Wludyka PS, Copeland KAF (2005) Analysis of Means: A Graphical Method for Comparing Means, Rates and Proportions. Asa Siam Ser Stat Ap 18: 1-247 Doi 10.1137/1.9780898718362
111 Newcombe VF, Williams GB, Outtrim JG, Chatfield D, Abate MG, Geeraerts T, Manktelow A, Room H, Mariappen L, Hutchinson PJet al (2013) Microstructural Basis of Contusion Expansion in Traumatic Brain Injury: Insights from Diffusion Tensor Imaging. Journal of Cerebral Blood Flow & Metabolism 33: 855-862 Doi 10.1038/jcbfm.2013.11
112 Ng SY, Lee AYW (2019) Traumatic Brain Injuries: Pathophysiology and Potential Therapeutic Targets. Frontiers in Cellular Neuroscience Volume 13 - 2019: Doi 10.3389/fncel.2019.00528
113 Nicholas AP, Sambandam T, Echols JD, Barnum SR (2005) Expression of citrullinated proteins in murine experimental autoimmune encephalomyelitis. The Journal of comparative neurology 486: 254-266 Doi 10.1002/cne.20527
114 Nielsen P, Olsen MH, Willer-Hansen RS, Hauerberg J, Johansen HK, Andersen AB, Knudsen JD, Møller K (2024) Ventriculostomy-associated infection (VAI) in patients with acute brain injury-a retrospective study. Acta neurochirurgica 166: 128 Doi 10.1007/s00701-024-06018-w
115 Nylén K, Ost M, Csajbok LZ, Nilsson I, Blennow K, Nellgård B, Rosengren L (2006) Increased serum-GFAP in patients with severe traumatic brain injury is related to outcome. Journal of the neurological sciences 240: 85-91 Doi 10.1016/j.jns.2005.09.007
116 Okonkwo DO, Puffer RC, Puccio AM, Yuh EL, Yue JK, Diaz-Arrastia R, Korley FK, Wang KKW, Sun X, Taylor SRet al (2020) Point-of-Care Platform Blood Biomarker Testing of Glial Fibrillary Acidic Protein versus S100 Calcium-Binding Protein B for Prediction of Traumatic Brain Injuries: A Transforming Research and Clinical Knowledge in Traumatic Brain Injury Study. Journal of neurotrauma 37: 2460-2467 Doi 10.1089/neu.2020.7140
117 Olabarria M, Goldman JE (2017) Disorders of Astrocytes: Alexander Disease as a Model. Annual Review of Pathology: Mechanisms of Disease 12: 131-152 Doi https://doi.org/10.1146/annurev-pathol-052016-100218
118 Pajares MA, Hernández-Gerez E, Pekny M, Pérez-Sala D (2023) Alexander disease: the road ahead. Neural Regen Res 18: 2156-2160 Doi 10.4103/1673-5374.369097
119 Papa L, Brophy GM, Welch RD, Lewis LM, Braga CF, Tan CN, Ameli NJ, Lopez MA, Haeussler CA, Mendez Giordano DIet al (2016) Time Course and Diagnostic Accuracy of Glial and Neuronal Blood Biomarkers GFAP and UCH-L1 in a Large Cohort of Trauma Patients With and Without Mild Traumatic Brain Injury. JAMA neurology 73: 551-560 Doi 10.1001/jamaneurol.2016.0039
120 Papa L, Lewis LM, Falk JL, Zhang Z, Silvestri S, Giordano P, Brophy GM, Demery JA, Dixit NK, Ferguson Iet al (2012) Elevated levels of serum glial fibrillary acidic protein breakdown products in mild and moderate traumatic brain injury are associated with intracranial lesions and neurosurgical intervention. Annals of emergency medicine 59: 471-483 Doi 10.1016/j.annemergmed.2011.08.021
121 Papa L, McKinley WI, Valadka AB, Newman ZC, Nordgren RK, Pramuka PE, Barbosa CE, Brito AMP, Loss LJ, Tinoco-Garcia Let al (2024) Diagnostic Performance of GFAP, UCH-L1, and MAP-2 Within 30 and 60 Minutes of Traumatic Brain Injury. JAMA Network Open 7: e2431115-e2431115 Doi 10.1001/jamanetworkopen.2024.31115
122 Pelinka LE, Kroepfl A, Leixnering M, Buchinger W, Raabe A, Redl H (2004) GFAP versus S100B in serum after traumatic brain injury: relationship to brain damage and outcome. Journal of neurotrauma 21: 1553-1561
123 Pereira JB, Janelidze S, Smith R, Mattsson-Carlgren N, Palmqvist S, Teunissen CE, Zetterberg H, Stomrud E, Ashton NJ, Blennow Ket al (2021) Plasma GFAP is an early marker of amyloid-β but not tau pathology in Alzheimer's disease. Brain : a journal of neurology 144: 3505-3516 Doi 10.1093/brain/awab223
124 Phillips CL, Faridounnia M, Armao D, Snider NT (2023) Stability dynamics of neurofilament and GFAP networks and protein fragments. Current opinion in cell biology 85: 102266 Doi 10.1016/j.ceb.2023.102266
125 Phillips CL, Fu D, Herring LE, Armao D, Snider NT (2022) Calpain-mediated proteolysis of vimentin filaments is augmented in giant axonal neuropathy fibroblasts exposed to hypotonic stress. Front Cell Dev Biol 10: 1008542 Doi 10.3389/fcell.2022.1008542
126 Pineda JA, Lewis SB, Valadka AB, Papa L, Hannay HJ, Heaton SC, Demery JA, Liu MC, Aikman JM, Akle Vet al (2007) Clinical significance of alphaII-spectrin breakdown products in cerebrospinal fluid after severe traumatic brain injury. Journal of neurotrauma 24: 354-366 Doi 10.1089/neu.2006.003789
127 Pohl C, Dikic I (2019) Cellular quality control by the ubiquitin-proteasome system and autophagy. Science 366: 818-822 Doi doi:10.1126/science.aax3769
128 Pruss RM (1985) Efficient detection of intermediate filament proteins using a panspecific monoclonal antibody: anti-IFA. Journal of neuroimmunology 8: 293-299 Doi 10.1016/s0165-5728(85)80068-0

129 Quinn JP, Corbett NJ, Kellett KAB, Hooper NM (2018) Tau Proteolysis in the Pathogenesis of Tauopathies: Neurotoxic Fragments and Novel Biomarkers. Journal of Alzheimer's Disease 63: 13-33 Doi 10.3233/jad-170959
130 Rai M, Curley M, Coleman Z, Nityanandam A, Jiao J, Graca FA, Hunt LC, Demontis F (2021) Analysis of proteostasis during aging with western blot of detergent-soluble and insoluble protein fractions. STAR Protoc 2: 100628 Doi 10.1016/j.xpro.2021.100628
131 Ringger NC, O'Steen BE, Brabham JG, Silver X, Pineda J, Wang KK, Hayes RL, Papa L (2004) A novel marker for traumatic brain injury: CSF alphaII-spectrin breakdown product levels. Journal of neurotrauma 21: 1443-1456
132 Robertson CS, Martinez FS, McQuillan LE, Williamson J, Lamb DG, Wang KKW, Rubenstein R, Wagner AK (2024) Serial Measurements of Serum Glial Fibrillary Acidic Protein in Moderate-Severe Traumatic Brain Injury: Potential Utility in Providing Insights into Secondary Insults and Long-Term Outcome. Journal of neurotrauma 41: 73-90 Doi 10.1089/neu.2023.0111
133 Rolleke U, Kumari P, Meyer R, Koster S (2023) The unique biomechanics of intermediate filaments - From single filaments to cells and tissues. Current opinion in cell biology 85: 102263 Doi 10.1016/j.ceb.2023.102263
134 Saatman KE, Creed J, Raghupathi R (2010) Calpain as a Therapeutic Target in Traumatic Brain Injury. Neurotherapeutics : the journal of the American Society for Experimental NeuroTherapeutics 7: 31-42 Doi https://doi.org/10.1016/j.nurt.2009.11.002
135 Sambandam T, Belousova M, Accaviti-Loper MA, Blanquicett C, Guercello V, Raijmakers R, Nicholas AP (2004) Increased peptidylarginine deiminase type II in hypoxic astrocytes. Biochemical and biophysical research communications 325: 1324-1329 Doi 10.1016/j.bbrc.2004.10.173
136 Sedmak G, Jovanov-Milošević N, Puskarjov M, Ulamec M, Krušlin B, Kaila K, Judaš M (2016) Developmental Expression Patterns of KCC2 and Functionally Associated Molecules in the Human Brain. Cerebral cortex 26: 4574-4589 Doi 10.1093/cercor/bhv218
137 Seidenfaden S-C, Kjerulff JL, Juul N, Kirkegaard H, Fogh Møller M, Bloch Münster A-M, Thingemann Bøtker M (2022) Temporal Changes in Serum S100B Levels From Prehospital to Early In-Hospital Sampling in Patients Suffering Traumatic Brain Injury. Frontiers in neurology Volume 13 - 2022: Doi 10.3389/fneur.2022.800015
138 Shi Y, Mowery RA, Ashley J, Hentz M, Ramirez AJ, Bilgicer B, Slunt-Brown H, Borchelt DR, Shaw BF (2012) Abnormal SDS-PAGE migration of cytosolic proteins can identify domains and mechanisms that control surfactant binding. Protein Sci 21: 1197-1209 Doi 10.1002/pro.2107
139 Shields DC, Tyor WR, Deibler GE, Hogan EL, Banik NL (1998) Increased calpain expression in activated glial and inflammatory cells in experimental allergic encephalomyelitis. Proceedings of the National Academy of Sciences 95: 5768-5772 Doi doi:10.1073/pnas.95.10.5768
140 Shin MK, Vazquez-Rosa E, Koh Y, Dhar M, Chaubey K, Cintron-Perez CJ, Barker S, Miller E, Franke K, Noterman MFet al (2021) Reducing acetylated tau is neuroprotective in brain injury. Cell 184: 2715-2732 e2723 Doi 10.1016/j.cell.2021.03.032
141 Shreiber DI, Bain AC, Ross DT, Smith DH, Gennarelli TA, McIntosh TK, Meaney DF (1999) Experimental investigation of cerebral contusion: histopathological and immunohistochemical evaluation of dynamic cortical deformation. Journal of neuropathology and experimental neurology 58: 153-164
142 Sofroniew MV, Vinters HV (2010) Astrocytes: biology and pathology. Acta Neuropathol 119: 7-35
143 Sosunov A, Olabarria M, Goldman JE (2018) Alexander disease: an astrocytopathy that produces a leukodystrophy. Brain pathology 28: 388-398 Doi 10.1111/bpa.12601
144 Stankewich MC, Cianci CD, Stabach PR, Ji L, Nath A, Morrow JS (2011) Cell organization, growth, and neural and cardiac development require αII-spectrin. Journal of cell science 124: 3956-3966 Doi 10.1242/jcs.080374
145 Strelkov SV, Herrmann H, Geisler N, Wedig T, Zimbelmann R, Aebi U, Burkhard P (2002) Conserved segments 1A and 2B of the intermediate filament dimer: their atomic structures and role in filament assembly. The EMBO journal 21: 1255-1266 Doi https://doi.org/10.1093/emboj/21.6.1255
146 Thelin EP, Zeiler FA, Ercole A, Mondello S, Buki A, Bellander BM, Helmy A, Menon DK, Nelson DW (2017) Serial Sampling of Serum Protein Biomarkers for Monitoring Human Traumatic Brain Injury Dynamics: A Systematic Review. Frontiers in neurology 8: 300 Doi 10.3389/fneur.2017.00300
147 Turtzo LC, Luby M, Jikaria N, Griffin AD, Greenman D, Bokkers RPH, Parikh G, Peterkin N, Whiting M, Latour LL (2021) Cytotoxic Edema Associated with Hemorrhage Predicts Poor Outcome after Traumatic Brain Injury. Journal of neurotrauma 38: 3107-3118 Doi 10.1089/neu.2021.0037
148 Vagberg M, Norgren N, Dring A, Lindqvist T, Birgander R, Zetterberg H, Svenningsson A (2015) Levels and Age Dependency of Neurofilament Light and Glial Fibrillary Acidic Protein in Healthy Individuals and Their Relation to the Brain Parenchymal Fraction. PloS one 10: e0135886 Doi 10.1371/journal.pone.0135886
149 Van Aelst S, Van Driessen K, Rousseeuw PJ (2000) A robust method for multivariate regression. St Class Dat Anal: 309-314
150 Verkhratsky A, Butt A, Li B, Illes P, Zorec R, Semyanov A, Tang Y, Sofroniew MV (2023) Astrocytes in human central nervous system diseases: a frontier for new therapies. Signal Transduct Target Ther 8: 396 Doi 10.1038/s41392-023-01628-9

151 Vespa P, Bergsneider M, Hattori N, Wu HM, Huang SC, Martin NA, Glenn TC, McArthur DL, Hovda DA (2005) Metabolic crisis without brain ischemia is common after traumatic brain injury: a combined microdialysis and positron emission tomography study. Journal of cerebral blood flow and metabolism : official journal of the International Society of Cerebral Blood Flow and Metabolism 25: 763-774 Doi 10.1038/sj.jcbfm.9600073
152 Vestling MM, Kelly MA, Fenselau C (1994) Optimization by mass spectrometry of a tryptophan-specific protein cleavage reaction. Rapid Commun Mass Spectrom 8: 786-790 Doi 10.1002/rcm.1290080925
153 Vlodavsky E, Palzur E, Shehadeh M, Soustiel JF (2017) Post-traumatic cytotoxic edema is directly related to mitochondrial function. Journal of cerebral blood flow and metabolism : official journal of the International Society of Cerebral Blood Flow and Metabolism 37: 166-177 Doi 10.1177/0271678X15621068
154 Wang B, Fields L, Li L (2023) Recent advances in characterization of citrullination and its implication in human disease research: From method development to network integration. Proteomics 23: e2200286 Doi 10.1002/pmic.202200286
155 Wanner IB (2012) An in vitro trauma model to study rodent and human astrocyte reactivity. Methods in molecular biology 814: 189-219 Doi 10.1007/978-1-61779-452-0_14
156 Weber JT (2012) Altered calcium signaling following traumatic brain injury. Frontiers in pharmacology 3: 60 Doi 10.3389/fphar.2012.00060
157 Whalen MJ, Dalkara T, You Z, Qiu J, Bermpohl D, Mehta N, Suter B, Bhide PG, Lo EH, Ericsson Met al (2008) Acute plasmalemma permeability and protracted clearance of injured cells after controlled cortical impact in mice. Journal of cerebral blood flow and metabolism : official journal of the International Society of Cerebral Blood Flow and Metabolism 28: 490-505 Doi 10.1038/sj.jcbfm.9600544
158 Wilde EA, Wanner IB, Kenney K, Gill J, Stone JR, Disner S, Schnakers C, Meyer R, Prager EM, Haas Met al (2022) A Framework to Advance Biomarker Development in the Diagnosis, Outcome Prediction, and Treatment of Traumatic Brain Injury. Journal of neurotrauma 39: 436-457 Doi 10.1089/neu.2021.0099
159 Wilson JE, Shinall MC, Jr., Leath TC, Wang L, Harrell FE, Jr., Wilson LD, Nordness MF, Rakhit S, de Riesthal MR, Duff MCet al (2021) Worse Than Death: Survey of Public Perceptions of Disability Outcomes After Hypothetical Traumatic Brain Injury. Ann Surg 273: 500-506 Doi 10.1097/SLA.0000000000003389
160 Wilson L, Newcombe VFJ, Whitehouse DP, Mondello S, Maas AIR, Menon DK, Ackerlund C, Amrein K, Andelic N, Andreassen Let al (2024) Association of early blood-based biomarkers and six-month functional outcomes in conventional severity categories of traumatic brain injury: capturing the continuous spectrum of injury. eBioMedicine 107: Doi 10.1016/j.ebiom.2024.105298
161 Wizeman JW, Nicholas AP, Ishigami A, Mohan R (2016) Citrullination of glial intermediate filaments is an early response in retinal injury. Mol Vis 22: 1137-1155
162 Xia Y, Lloyd GM, Giasson BI (2021) Targeted proteolytic products of τ and α-synuclein in neurodegeneration. Essays Biochem 65: 905-912 Doi 10.1042/ebc20210028
163 Xiong G, Elkind JA, Kundu S, Smith CJ, Antunes MB, Tamashiro E, Kofonow JM, Mitala CM, Cole J, Stein SCet al (2014) Traumatic brain injury-induced ependymal ciliary loss decreases cerebral spinal fluid flow. Journal of neurotrauma 31: 1396-1404 Doi 10.1089/neu.2013.3110
164 Xiong L, Sun L, Liu S, Zhu X, Teng Z, Yan J (2019) The Protective Roles of Urinary Trypsin Inhibitor in Brain Injury Following Fat Embolism Syndrome in a Rat Model. Cell Transplant 28: 704-712 Doi 10.1177/0963689718814766
165 Yamal JM, Aisiku IP, Hannay HJ, Brito FA, Robertson CS (2021) Disability Rating Scale in the First Few Weeks After a Severe Traumatic Brain Injury as a Predictor of 6-Month Functional Outcome. Neurosurgery 88: 619-626 Doi 10.1093/neuros/nyaa474
166 Yang Z, Arja RD, Zhu T, Sarkis GA, Patterson RL, Romo P, Rathore DS, Moghieb A, Abbatiello S, Robertson CSet al (2022) Characterization of Calpain and Caspase-6-Generated Glial Fibrillary Acidic Protein Breakdown Products Following Traumatic Brain Injury and Astroglial Cell Injury. International Journal of Molecular Sciences 23: 8960
167 Yap YW, Whiteman M, Bay BH, Li Y, Sheu FS, Qi RZ, Tan CH, Cheung NS (2006) Hypochlorous acid induces apoptosis of cultured cortical neurons through activation of calpains and rupture of lysosomes. Journal of neurochemistry 98: 1597-1609 Doi 10.1111/j.1471-4159.2006.03996.x
168 Yeh P-H, Lippa SM, Brickell TA, Ollinger J, French LM, Lange RT (2022) Longitudinal changes of white matter microstructure following traumatic brain injury in U.S. military service members. Brain Communications 4: Doi 10.1093/braincomms/fcac132
169 Zhang A, Zhang Z, Liu Y, Lenahan C, Xu H, Jiang J, Yuan L, Wang L, Xu Y, Chen Set al (2022) The Role of Caspase Family in Acute Brain Injury: The Potential Therapeutic Targets in the Future. Current neuropharmacology 20: 1194-1211 Doi 10.2174/1570159x19666211111121146
170 Zhao X, Ahram A, Berman RF, Muizelaar JP, Lyeth BG (2003) Early loss of astrocytes after experimental traumatic brain injury. Glia 44: 140-152 Doi 10.1002/glia.10283
171 Zhou Z, Zhao T, Gardus J, Wen Q, Feng Y, DeLorenzo C, Parsey R, Huang C (2025) Quantifying Ventricular CSF Clearance in the Human Brain Using Dynamic 18F-FDG PET: Insights into Age-Related Glymphatic Impairment. medRxiv: 2025.2004.2007.25325241 Doi 10.1101/2025.04.07.25325241

172 Zhu X, Tao L, Tejima-Mandeville E, Qiu J, Park J, Garber K, Ericsson M, Lo EH, Whalen MJ (2012) Plasmalemma permeability and necrotic cell death phenotypes after intracerebral hemorrhage in mice. Stroke; a journal of cerebral circulation 43: 524-531 Doi 10.1161/STROKEAHA.111.635672
173 Zoltewicz JS, Mondello S, Yang B, Newsom KJ, Kobeissy F, Yao C, Lu XC, Dave JR, Shear DA, Schmid Ket al (2013) Biomarkers track damage after graded injury severity in a rat model of penetrating brain injury. Journal of neurotrauma 30: 1161-1169 Doi 10.1089/neu.2012.2762

DECLARATIONS

Ethics approval and consent to participate

For deidentified TBI patient's CSF and serum collection with metadata, adult patients (>18 years of age) were enrolled at two Level 1 trauma centers, in Los Angeles, California, at the UCLA Ronald Reagan Hospital Neuro-Intensive Care Unit, and in Gainesville, Florida (UF Health Shands Hospital, University of Florida). The human subjects' protocols included local IRBs that approved informed consent procedures at UCLA under Chair Paul Vespa and at the University of Florida Dept of Anesthesiology under Steven Robicsek, Md, PhD. The Study "Biochemical markers for traumatic brain injury tissue and data bank" was approved by the Institutional Review Board (IRB) of the University of Florida with the IRB# 201703310. Patients met inclusion criteria if they were 18 years old with a non-penetrating head injury and had a GCS <8 requiring the placement of an intraventricular catheter. Patients were excluded if they had a history of preexisting end-stage organ disease or severe psychiatric illness. At UCLA, the Office for Human Research Protection (OHRP) approved the informed consent protocol for the Brain Injury Research Center study with the BIRC-IRB# 10-0929.

The UCLA Office for Protection of Research Subject (OPRS) declared IRB exemption status for deidentified pre-shelved fetal brain specimen donation per HS-7 exemption amendment. Deidentified human fetal brain tissue from voluntarily aborted pregnancies was donated adhering to stringent ethical regulations. Tissue was preshelved at the UCLA Translational Pathology Core Laboratory (Sara Dry, Chair of Pathology and Laboratory Medicine). Consent was established through UCLA Dept of OB-GYN (Angela Chen, Division Chief of Family Planning). Signed informed consent occurred after decision on elective termination, complying with US Public Law 103-43 and NIH policy, ensuring no incentive (The Public Health Service Act, 42 U.S.C. § 289g-2).

Consent for publication

This manuscript contains no individual personal information, so individual consent for publication is not applicable.

Availability of data and materials

The datasets supporting the conclusions of this article are included within the article and its additional files with file names listed under Additional material. The CSF GFAP and BDPs longitudinal quantification

dataset of 24 TBI patients is freely accessible through the Open Data Commons for Traumatic Brain Injury repository (ODC-TBI), under the Wanner lab space with data dictionary, the unique persistent identifier, the hyperlink to this dataset is provided here: https://odc-tbi.org/lab/dataset?labid=387&datasetid=1432.

Mass spectrometry raw data of GFAP fragments' peptide sequence PD files and label-free peptide/ion quantification of four TBI patients (six CSF samples) are publicly accessible at the Center for Computational Mass Spectrometry (CCMS) ProteoSAFe (Proteomics Software Environment) web server as a MassIVE (MS Interactive Virtual Environment) file folder provided here:

https://massive.ucsd.edu/ProteoSAFe/dataset.jsp?task=460f951a666a4b599df2bfa37fa33fbd.

FIGURES & SUPPLEMENTS

This manuscript includes a file with eight figures called '*Figures-GFAP-trauma-Wanner'*. A supplement is included, which contains 14 Additional Figures (labeled Figures S1-S14) and eight Tables S1-S8 that are compiled into one pdf file called '*Supplement-GFAP-trauma-Wanner'*. Further, complete and uncropped immunoblot images of the figures are provided in *'GFAP-uncropped blots-Supplementary-Wanner'*.

COMPETING INTEREST INFORMATION

IBW and **JAL** are inventors of the following patents licensed to BRAINBox Solutions Inc., where **TVM** serves as Chief Scientific Officer (CSO). **GS** is CEO and founder of EnCor Biotechnology Inc., which distributes several monoclonal GFAP antibodies used in this study.
US Patent Issue No.: US 10,557,859 B2 original patent; Inventors I.B. Wanner and J.A. Loo, Issue date: 2/11/2020; 25 claims prior publication 12/20/2018: "Astrocyte traumatome and neurotrauma biomarkers".
Applicant Regents of the University of California, Oakland, CA. Licensee: BRAINBox Solutions Inc.
US Issue No.: US 11,249,094 B2 Additional 13 claims in divisional patent 13 Claims, Filed 12/116/2019; Issue date: 2/15/2022; Inventors: Wanner and Loo, UCLA "Astrocyte traumatome and neurotrauma biomarkers". Assignee UCLA; Licensee: Brain Box Solutions Inc.

AUTHOR CONTRIBUTION INFORMATION

IBW conceptualized and designed the study, wrote and revised the manuscript, curated data and conducted formal analysis, designed and prepared all visualizations, acquired funding, coordinated research activities, supervised laboratory assistants and students and conducted cell culture and live cell imaging studies. **JH** and **JL** conducted sample preparation and immunological experiments, assembled raw data and illustrations, curated and analyzed data. **JL, SS** and **YC** analyzed MS spectra. **YC** and **SS** conducted MS analyses. **HZ** provided the thumbnail infographic. **CS** analyzed data and provided visualizations. **ROL** and **JAL** provided MS data analysis guidance and **JAL** was involved in the study conceptualization. **TVM** and **GS** provided antibodies, peptides and recombinant proteins, assisted in writing the manuscript and offered biochemical guidance. **GS** also conducted antibody binding and chemical cleavage studies and wrote the structural part of the discussion. **BME** provided data interpretation and manuscript revision. **JG** provided guidance on data curation and statistical analysis approaches. **SR** and **PMV** had oversight over clinical aspects of the study including TBI patient enrollment, IRB approval and sample provision. Further, **PMV** provided guidance, manuscript organization and contributed to written content and clinical interpretation of the findings. Resources included **IDDRC** laboratory infrastructure including cell culture, centrifuges, gel imagers. The **MIC**

provided mass spectrometry instruments and proteomics facilities for the study. ***All authors*** *read, reviewed, edited and approved of the final manuscript.*

Thumbnail

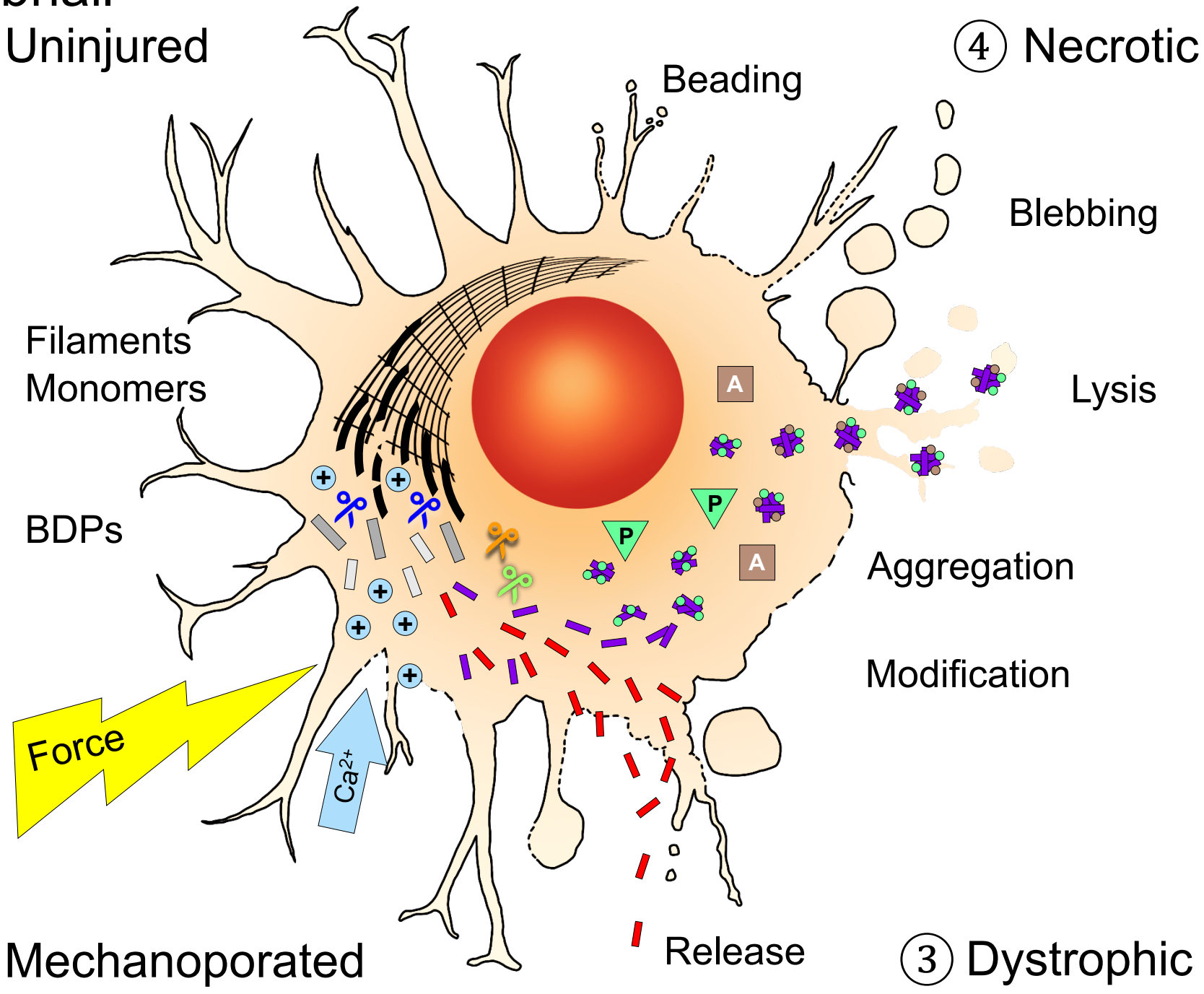

Symbol key

- GFAP Filaments
- GFAP Monomers +/- break
- Large GFAP-BDPs (42-49kDa)
- Calpain GFAP-BDPs (37-39kDa)
- Small GFAP Coil1-BDPs
- Small GFAP Coil2-BDPs
- GFAP Aggregates
- Calcium
- Peptidyl deiminases, PADs
- Citrullination
- Acetyltransferases
- Acetylation
- Calpain
- Caspase
- Endogenous Trypsin activity

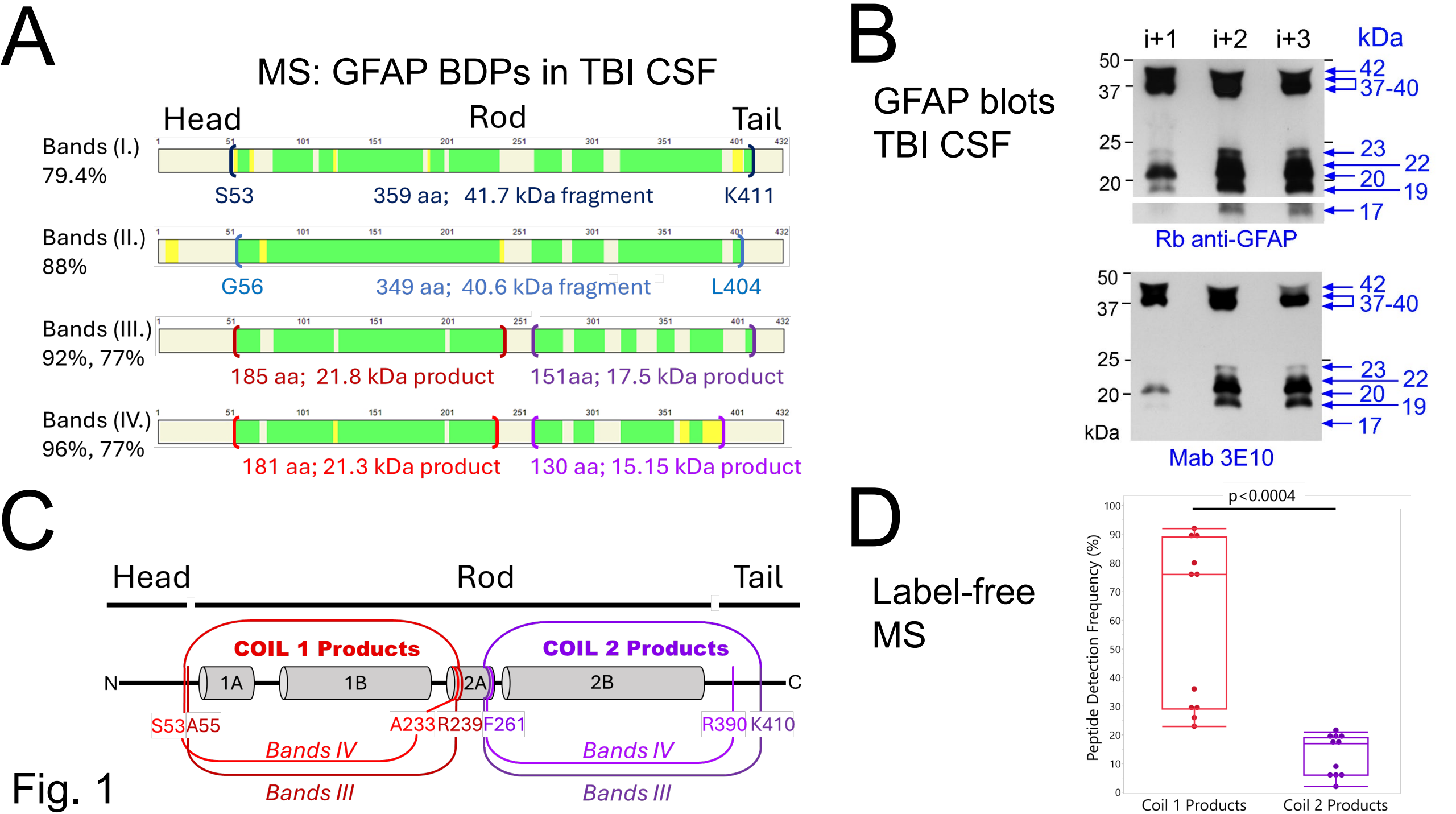
A
MS: GFAP BDPs in TBI CSF
Head
Rod
Tail
Bands (I.)
79.4%
S53
359 aa; 41.7 kDa fragment
K411
Bands (II.)
88%
G56
349 aa; 40.6 kDa fragment
L404
Bands (III.)
92%, 77%
185 aa; 21.8 kDa product
151aa; 17.5 kDa product
Bands (IV.)
96%, 77%
181 aa; 21.3 kDa product
130 aa; 15.15 kDa product
B
GFAP blots
TBI CSF
i+1
i+2
i+3
kDa
50
37
25
20
42
37-40
23
22
20
19
17
Rb anti-GFAP
Mab 3E10
C
Head
Rod
Tail
COIL 1 Products
COIL 2 Products
N
1A
1B
2A
2B
C
S53
A55
A233
R239
F261
R390
K410
Bands IV
Bands III
D
Label-free
MS
p<0.0004
Peptide Detection Frequency (%)
Coil 1 Products
Coil 2 Products

Fig. 1

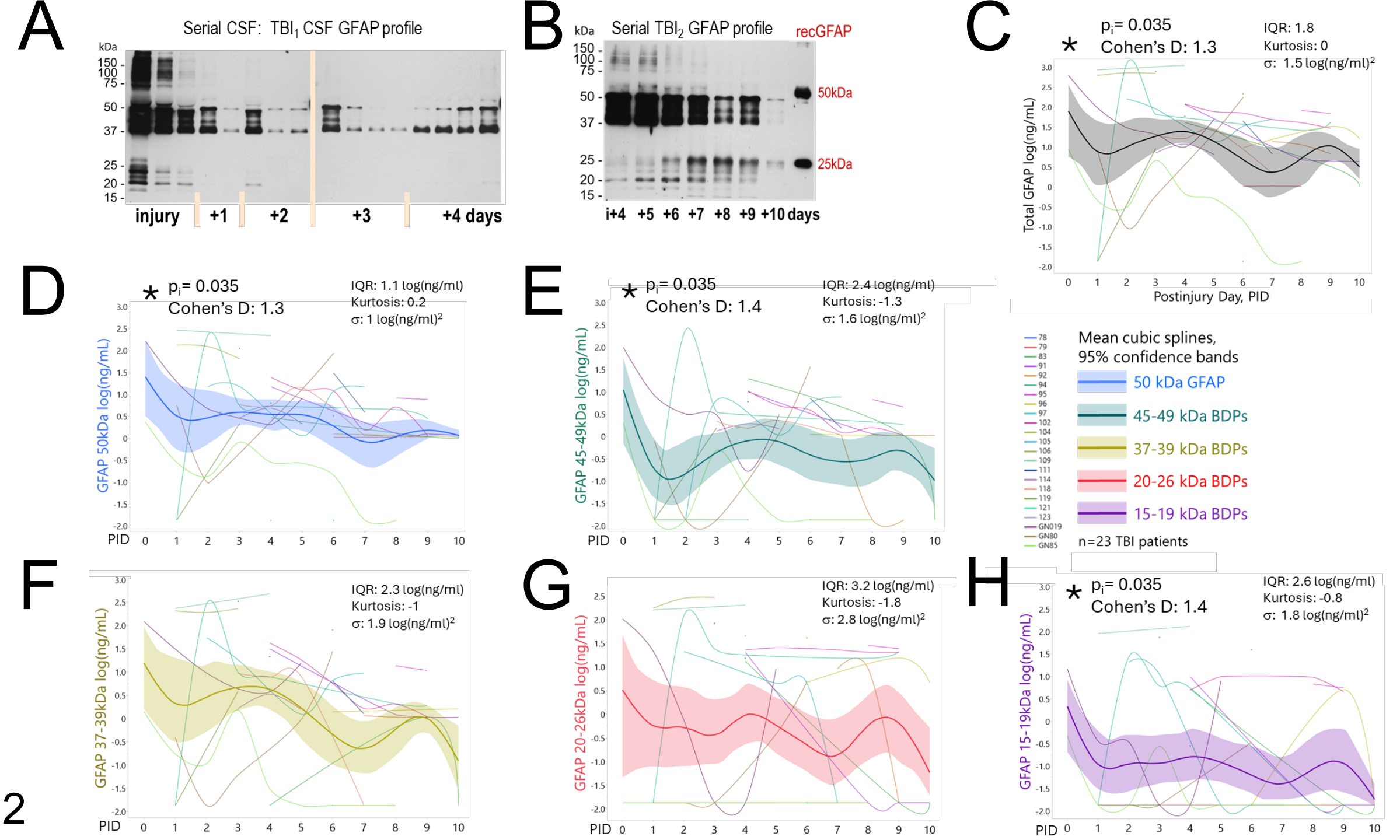
A
Serial CSF: TBI1 CSF GFAP profile
kDa
150
100
75
50
37
25
20
15
injury
+1
+2
+3
+4 days
B
Serial TBI2 GFAP profile
recGFAP
50kDa
25kDa
i+4 +5 +6 +7 +8 +9 +10 days
C
* pi= 0.035
Cohen's D: 1.3
IQR: 1.8
Kurtosis: 0
σ: 1.5 log(ng/ml)2
Total GFAP log(ng/mL)
Postinjury Day, PID
D
* pi= 0.035
Cohen's D: 1.3
IQR: 1.1 log(ng/ml)
Kurtosis: 0.2
σ: 1 log(ng/ml)2
GFAP 50kDa log(ng/mL)
PID
E
* pi= 0.035
Cohen's D: 1.4
IQR: 2.4 log(ng/ml)
Kurtosis: -1.3
σ: 1.6 log(ng/ml)2
GFAP 45-49kDa log(ng/mL)
PID
Mean cubic splines,
95% confidence bands
50 kDa GFAP
45-49 kDa BDPs
37-39 kDa BDPs
20-26 kDa BDPs
15-19 kDa BDPs
n=23 TBI patients
F
IQR: 2.3 log(ng/ml)
Kurtosis: -1
σ: 1.9 log(ng/ml)2
GFAP 37-39kDa log(ng/mL)
PID
G
IQR: 3.2 log(ng/ml)
Kurtosis: -1.8
σ: 2.8 log(ng/ml)2
GFAP 20-26kDa log(ng/mL)
PID
H
* pi= 0.035
Cohen's D: 1.4
IQR: 2.6 log(ng/ml)
Kurtosis: -0.8
σ: 1.8 log(ng/ml)2
GFAP 15-19kDa log(ng/mL)
PID

Fig. 2

A

Pearsons Correlation Coefficients

	45-49kDa	40-42kDa	37-39kDa	20-26kDa	15-19kDa
50kDa	0.575	0.637	0.822	0.604	0.529
45-49kDa		0.596	0.589	0.413	0.422
40-42kDa			0.726	0.549	0.363
37-39kDa				0.714	0.567
20-26kDa					0.685
15-19kDa					

B

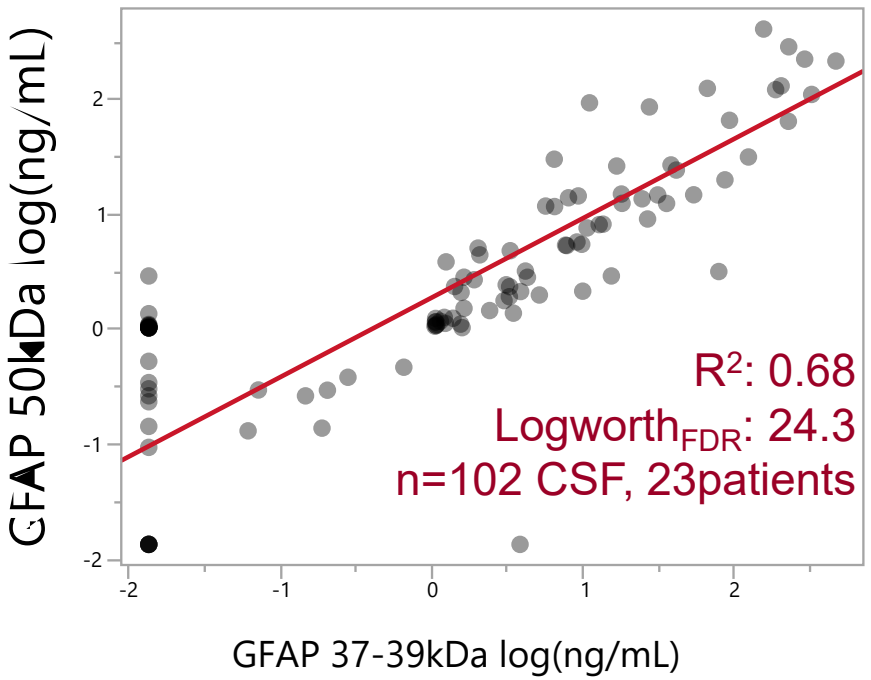

C

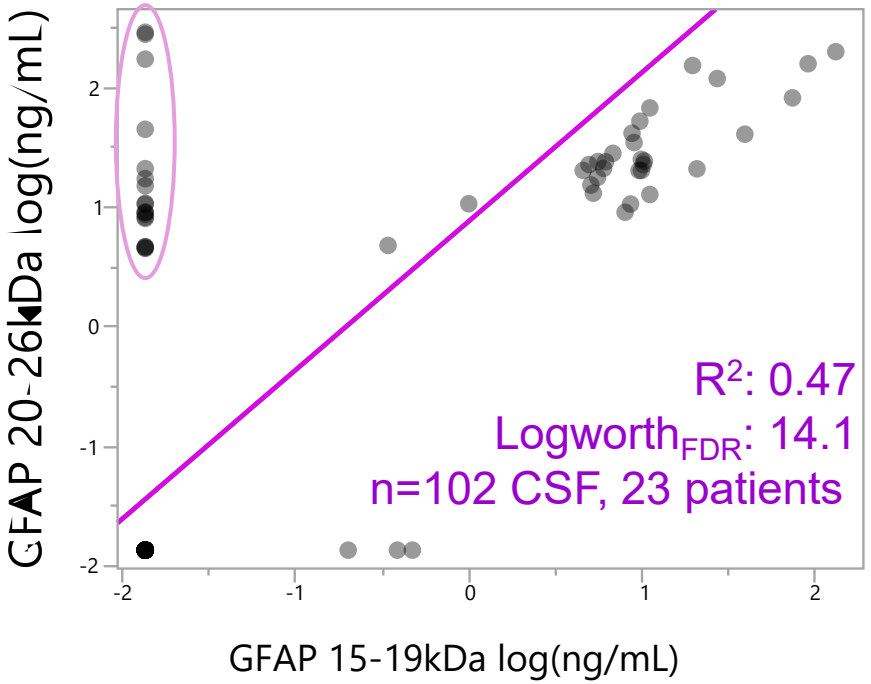

Fig. 3

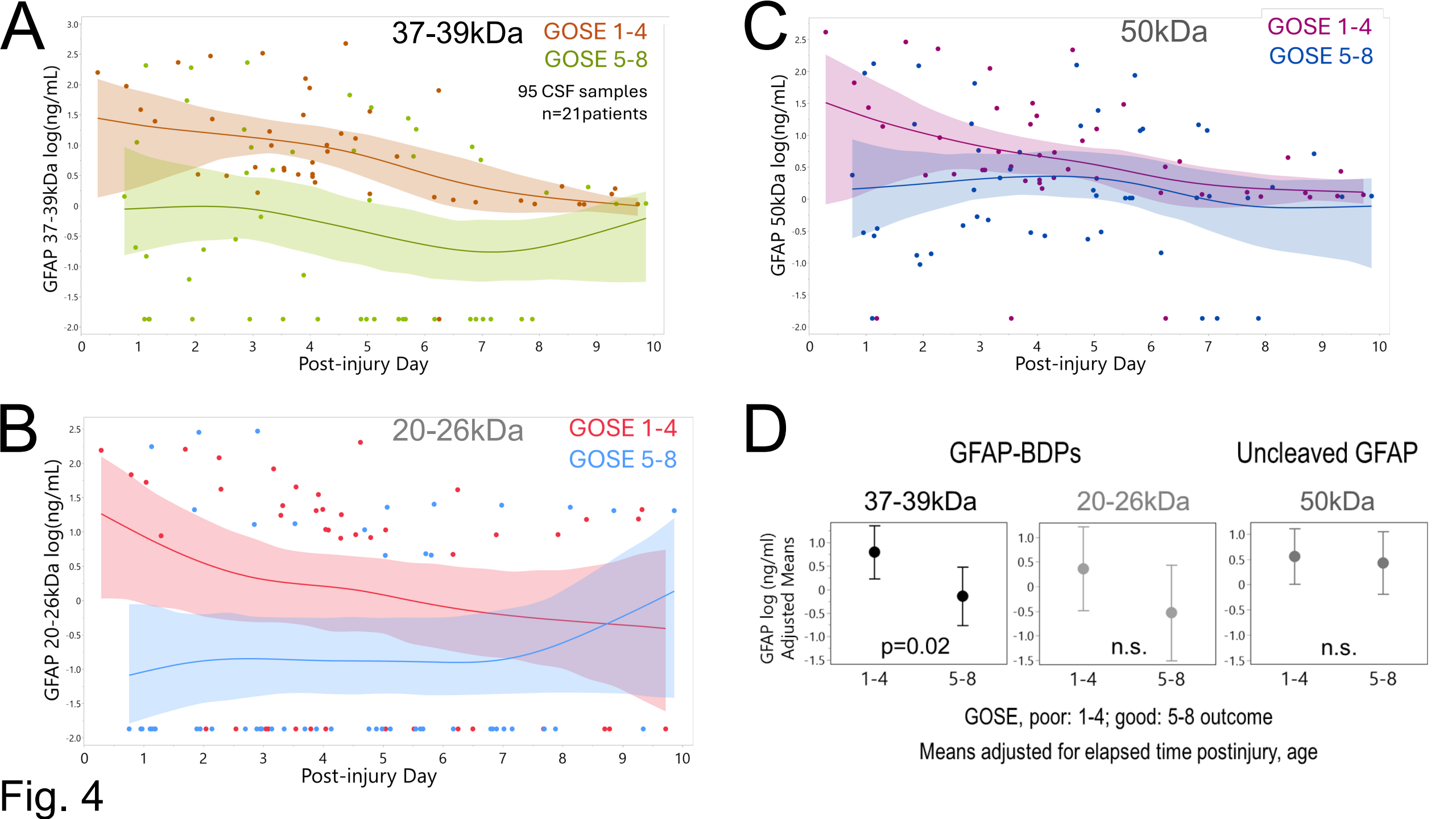
A
37-39kDa
GOSE 1-4
GOSE 5-8
95 CSF samples
n=21patients
GFAP 37-39kDa log(ng/mL)
Post-injury Day
C
50kDa
GOSE 1-4
GOSE 5-8
GFAP 50kDa log(ng/mL)
Post-injury Day
B
20-26kDa
GOSE 1-4
GOSE 5-8
GFAP 20-26kDa log(ng/mL)
Post-injury Day
D
GFAP-BDPs
Uncleaved GFAP
37-39kDa
20-26kDa
50kDa
GFAP log (ng/ml)
Adjusted Means
p=0.02
n.s.
n.s.
1-4
5-8
GOSE, poor: 1-4; good: 5-8 outcome
Means adjusted for elapsed time postinjury, age

Fig. 4

A

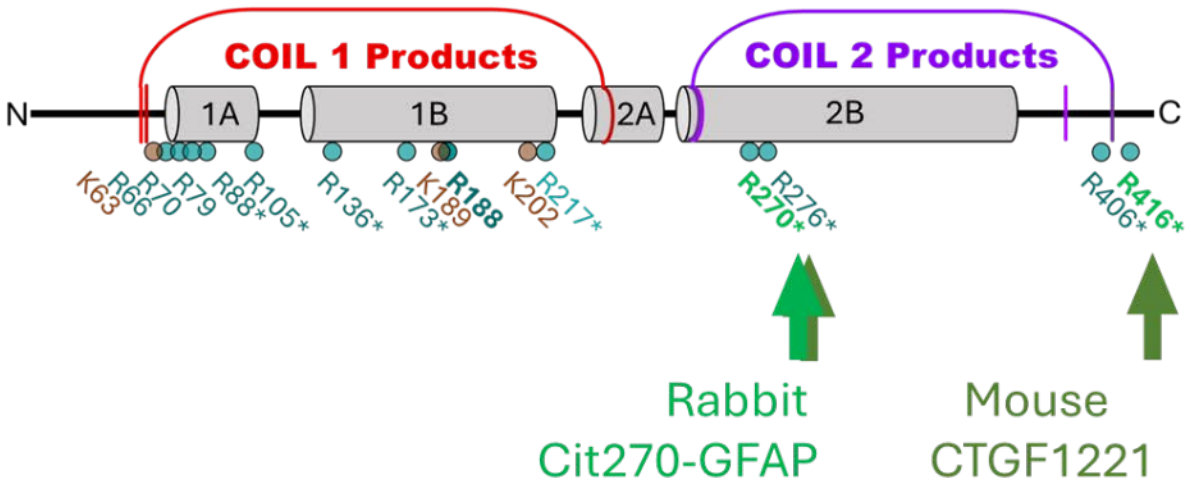

13 Citrullinated arginine residues

5 Acetylated lysine residues

B

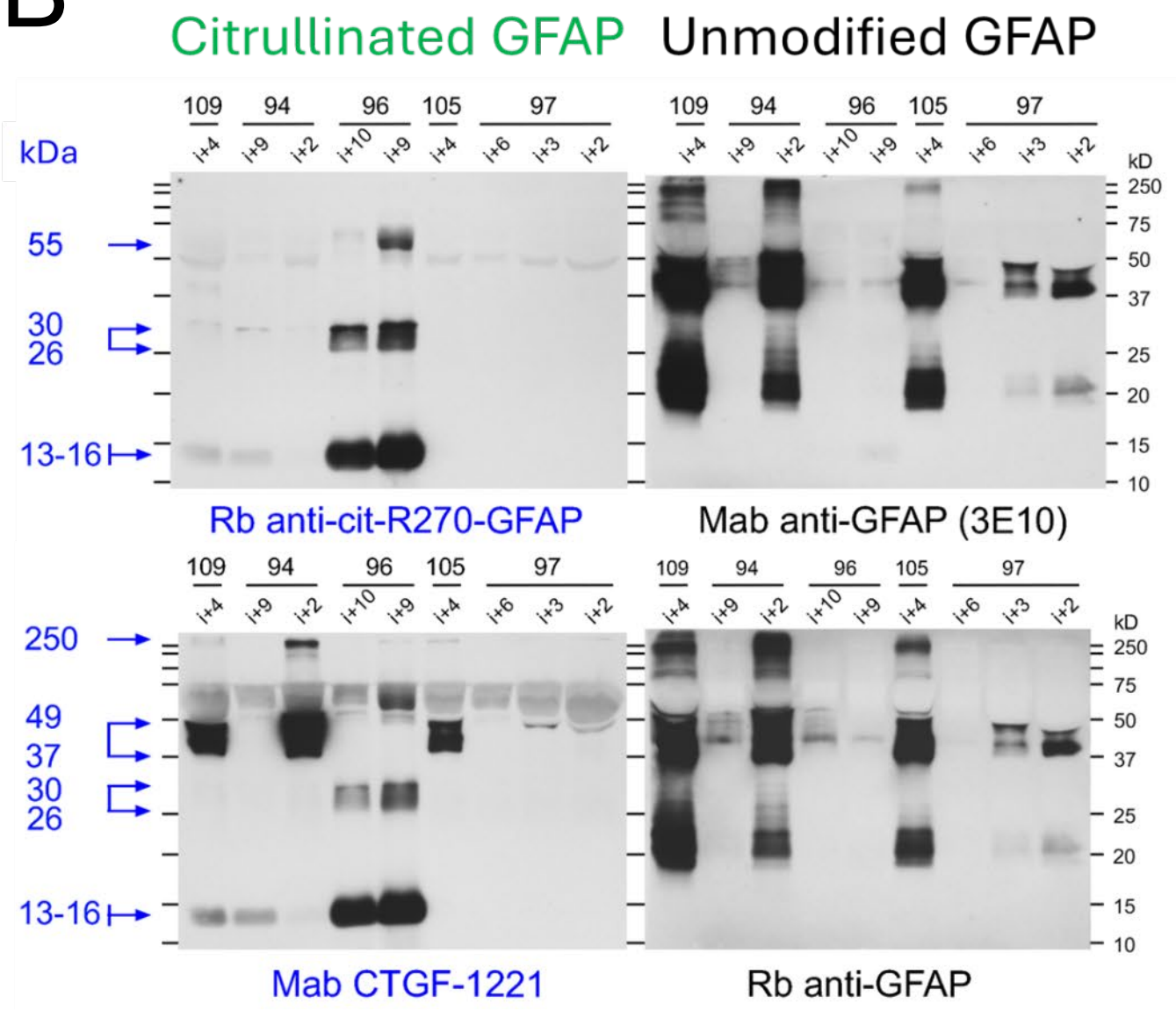

Fig. 5

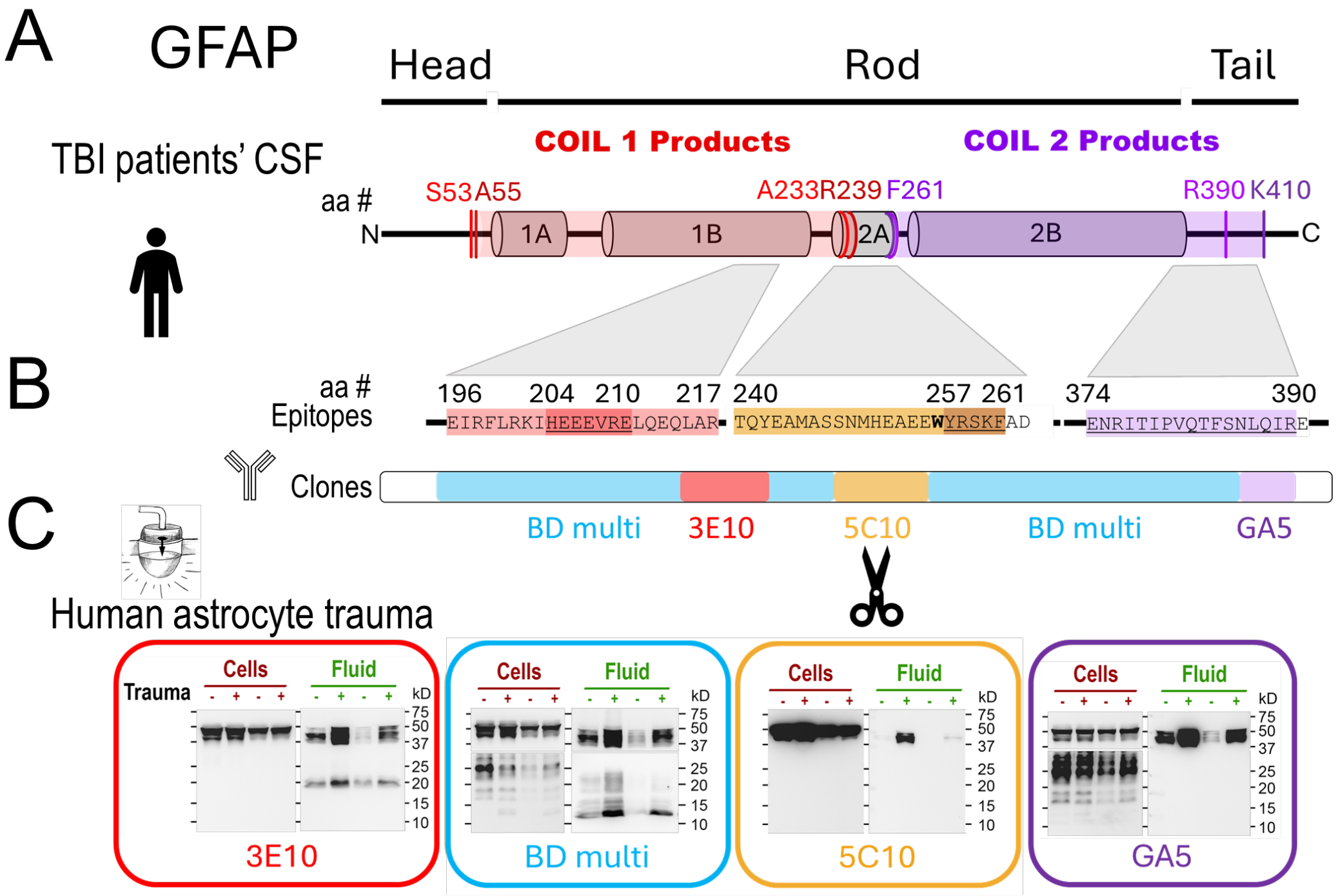
A
GFAP
Head
Rod
Tail
TBI patients' CSF
COIL 1 Products
COIL 2 Products
aa #
S53A55
A233R239
F261
R390
K410
N
1A
1B
2A
2B
C
B
aa #
196
204
210
217
240
257
261
374
390
Epitopes
EIRFLRKIHEEEVRELQEQLAR
TQYEAMASSNMHEAEEWYRSKFAD
ENRITIPVQTFSNLQIRE
Clones
BD multi
3E10
5C10
BD multi
GA5
C
Human astrocyte trauma
Trauma
Cells
Fluid
kD
75
50
37
25
20
15
10
3E10
BD multi
5C10
GA5

Fig. 6

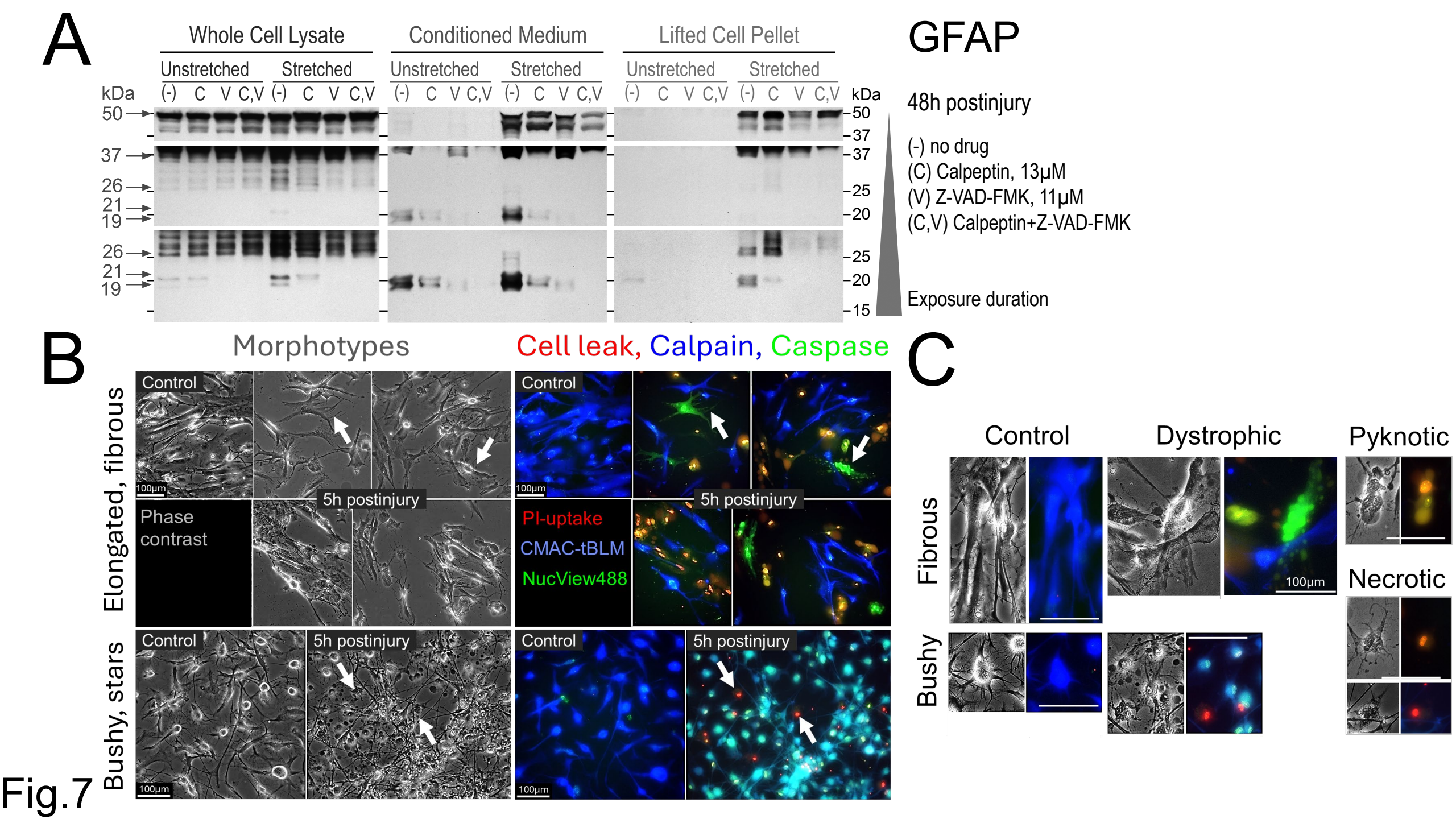
A
GFAP
Whole Cell Lysate
Conditioned Medium
Lifted Cell Pellet
Unstretched
Stretched
kDa
(-) C V C,V
50
37
26
21
19
25
20
15
48h postinjury
(-) no drug
(C) Calpeptin, 13μM
(V) Z-VAD-FMK, 11μM
(C,V) Calpeptin+Z-VAD-FMK
Exposure duration
B
Morphotypes
Cell leak, Calpain, Caspase
Elongated, fibrous
Bushy, stars
Control
5h postinjury
Phase contrast
PI-uptake
CMAC-tBLM
NucView488
100μm
C
Control
Dystrophic
Pyknotic
Necrotic
Fibrous
Bushy
100μm

Fig.7

A

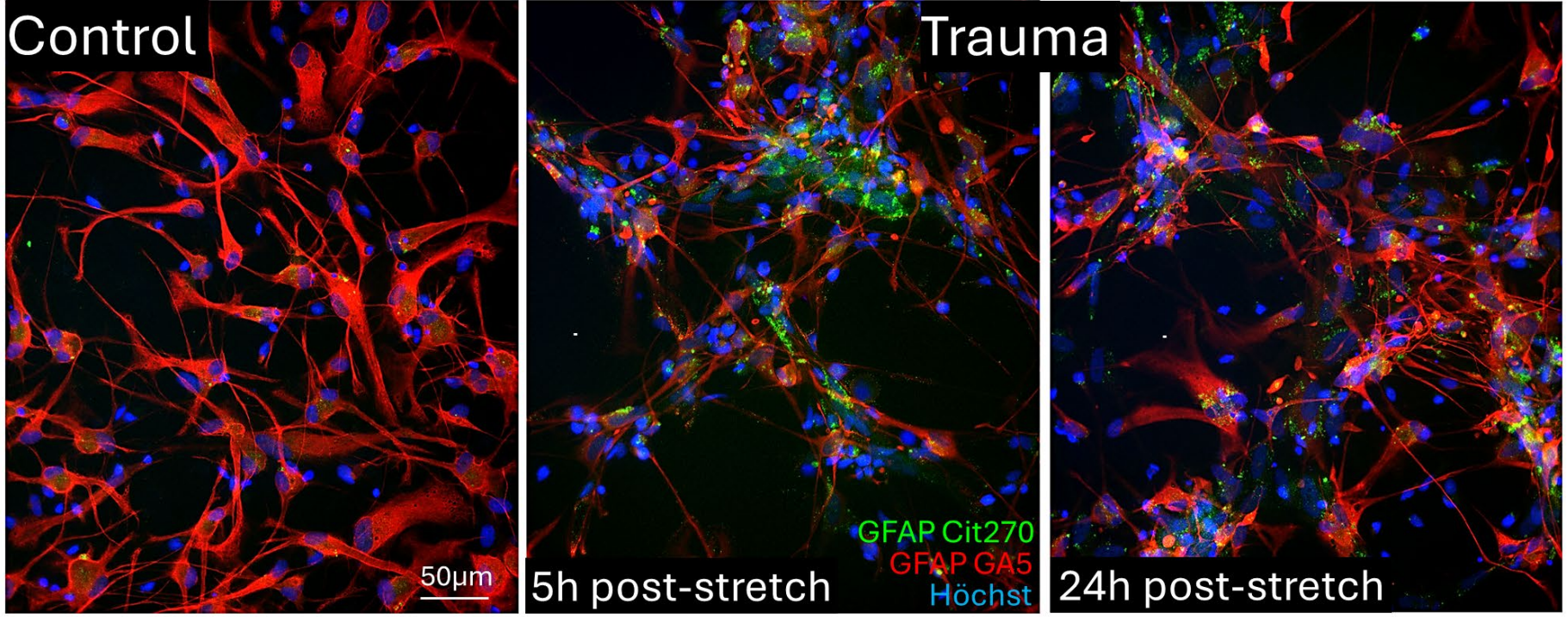
Control
Trauma
50µm
5h post-stretch
GFAP Cit270
GFAP GA5
Höchst
24h post-stretch

B

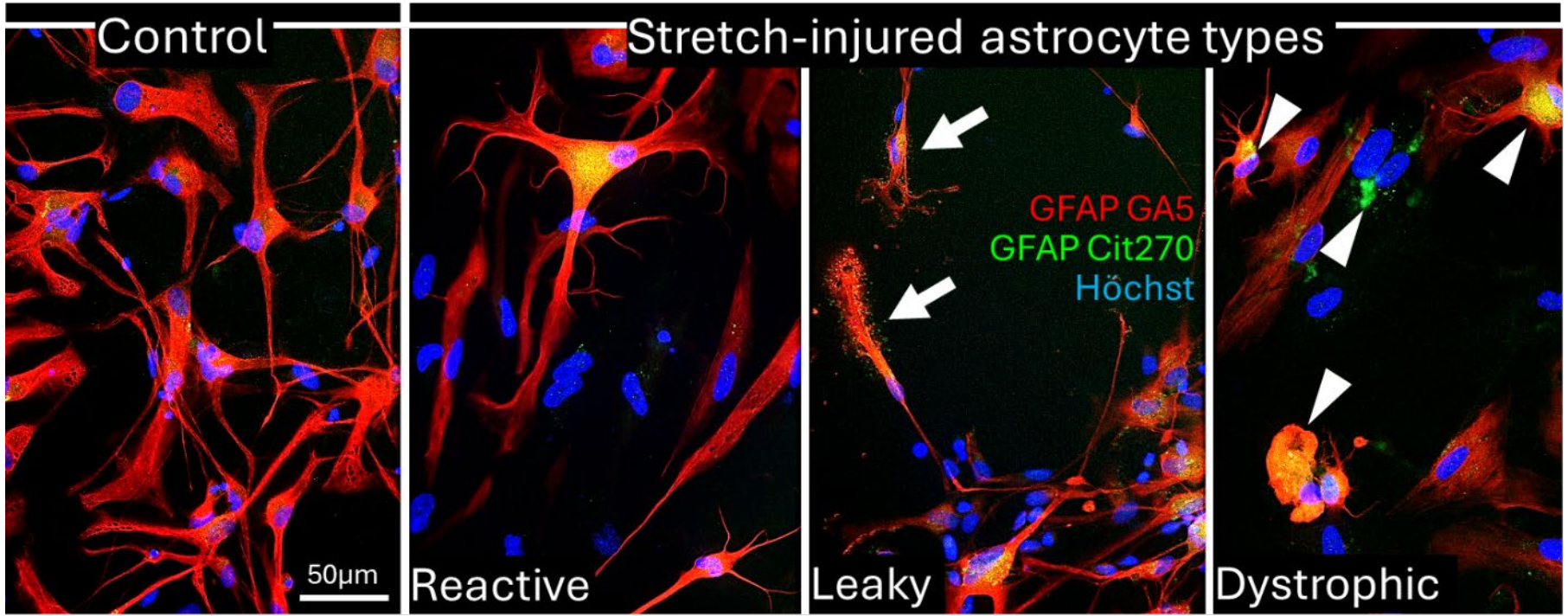
Control
Stretch-injured astrocyte types
50µm
Reactive
GFAP GA5
GFAP Cit270
Höchst
Leaky
Dystrophic

Fig. 8